Science

RESEARCH ARTICLES

Cite as: M. Wiesbeck *et al.*, *Science* 10.1126/science.aeh1348 (2026).

# Manipulation of protein translation and stem cell self-renewal by CRISPR activation of rRNA transcription

**Maximilian Wiesbeck[1,2], Emilie L. Alard[3], Florencia Merino[1,2,4,†], Niti Chowdhury[5,6,7], Luisa Egert[2], Anna Danese[1,8], Simon Imhof[1], Matilde Iraci Borgia[1,4], Akshaya Rajan[1,4,‡], Nadine Fernandez-Novel Marx[1], Edina Kepesidis[2], Anna Köferle[1§], Luis Miguel Cerron-Alvan[1¶], Franziska Vierl[2,1,4], Thi-Tram Truong[1,2], Manja Thorwirth[2,1], Lorina Bilalli[9], Jovica Ninkovic[10,8], Rico Schieweck[9], Markus Diefenbacher[5,6,7], Stefanie M. Hauck[11], Paul Trainor[12,13], Faraz K. Mardakheh[3], Magdalena Götz[1,2,14], Stefan H. Stricker[1,2*]**

[1]Division of Physiological Genomics, Biomedical Center (BMC), LMU Medizin, Ludwig-Maximilians-Universität München, Planegg-Martinsried, Germany. [2]Institute of Stem Cell Research, Helmholtz Zentrum, German Research Center for Environmental Health, Planegg-Martinsried, Germany. [3]Department of Biochemistry, University of Oxford, Oxford, UK. [4]Graduate School of Systemic Neurosciences, LMU Medizin, Ludwig-Maximilians-Universität München, Planegg-Martinsried, Germany. [5]Institute of Lung Health and Immunity (LHI), Helmholtz Munich, Comprehensive Pneumology Center (CPC-M), Member of the German Center for Lung Research (DZL), Neuherberg, Germany. [6]Institute of Experimental Pneumology, LMU Klinikum, LMU Medizin, Ludwig-Maximilians-Universität München, Munich, Germany. [7]German Cancer Research Center (DKTK) Munich, Munich, Germany. [8]Research Unit Central Nervous System Regeneration, Helmholtz Zentrum, Munich, Germany. [9]Luxembourg Centre for Systems Biomedicine (LCSB), University of Luxembourg, Esch-sur-Alzette, Luxembourg. [10]Department for Cell Biology and Anatomy, Biomedical Center (BMC), LMU Medizin, Ludwig-Maximilians-Universität München, Planegg-Martinsried, Germany. [11]Metabolomics and Proteomics Core, Helmholtz Centre Munich, German Research Center for Environmental Health, Neuherberg, Germany. [12]Stowers Institute for Medical Research, Kansas City, MO, USA. [13]Department of Cell Biology and Physiology, The University of Kansas Medical Center, Kansas City, KS, USA. [14]Excellence Cluster of Systems Neurology (SYNERGY), Munich, Germany.

***Corresponding author. Email: stefan.stricker@med.uni-muenchen.de**

†Present address: Department of Basic Neurosciences, University of Geneva, Geneva, Switzerland.

‡Present address: Arc Institute, Palo Alto, CA, USA.

§Present address: Boehringer Ingelheim RCV GmbH & Co KG, Vienna, Austria.

¶Present address: Max Perutz Labs, Vienna BioCenter, Vienna, Austria.

**Ribosomal RNA (rRNA) transcription rates vary during development, and their dysregulation is linked to diseases such as cancer and ribosomopathies. Owing to their high abundance and genomic redundancy, the functional significance of rRNA-levels remains unclear. Here, we developed TAPIR (Targeted Activation of Protein Translation), a CRISPR-based approach to elevate rRNA-levels by inducing 47S rDNA transcription. TAPIR increased nucleolar size and enhanced protein synthesis, even in rapidly proliferating cells. In neural stem cells, elevated translation promoted self-renewal and proliferation in vitro and in vivo. Furthermore, TAPIR enabled the modeling and partial rescue of associated disease phenotypes. Our findings revealed that rRNA-levels directly regulate translational output and that protein synthesis capacity can act as a key determinant of mammalian stem cell behavior.**

The activity of protein synthesis rates vary widely between cell types, but how these differences are controlled and how important they are remains unclear (*1*). Most insights come from studies of growth-related signaling pathways regulating cellular growth beyond protein translation rates (such as mTOR) and factors that regulate subsets of mRNAs, including translation initiation factors, RNA-binding proteins, and non-coding RNAs. Little attention has been paid to the regulatory roles of core ribosomal components, particularly ribosomal RNA (rRNA), despite its essential and ubiquitous function in protein synthesis. rRNAs are the predominant transcripts in the cell, accounting for 70-80% of cellular RNA and 35-60% of all ongoing transcription in cycling cells (*2*). Three of the four eukaryotic rRNAs (18S, 5.8S, and 28S) are processed from a single progenitor (pre-rRNA or 45S), which is transcribed by RNA Pol I from the rDNA as a slightly longer template (47S). The number of 47S rDNA genes can vary in eukaryotes by almost one order of magnitude (150-1000); they are, however, consistently organized in the form of repetitive arrays (*3–5*). The nucleolus is a nuclear organelle where rRNA transcription, rRNA processing, and ribosome assembly occur (*3*, *6*). In mammals, a typical rDNA array contains 30-40 47S genes and occupies a number of genomic loci, the nucleolar organizing regions (NORs) (Fig. 1A), which macroscopically form the nucleolus.

The number and size of nucleoli vary between cell types and tissues, as does the fraction of rDNA genes that is actively transcribed. Even fast dividing cells, such as yeast or cancer cell lines, which express high levels of rRNA, use only 50% of their rDNA genes at any one time (*4*), whereas quiescent, senescent, slowly cycling or metabolically restricted cells are believed to use significantly fewer (*7*). Balanced regulation of

rRNA expression and/or protein translation rates has been noted in a series of fundamental biological processes [e.g., cellular differentiation (*8*–*10*), cell size regulation (*11*) and cell proliferation (*10*)]. Its perturbation is apparent in a number of human conditions [e.g., cancer (*12*–*15*), neurodegenerative and neurodevelopmental diseases (*16*–*19*), ribosomopathies and aging (*6*, *20*–*24*)].

However, it remains unclear whether rRNAs level directly regulate these processes and are viable therapeutic targets, or instead reflect secondary effects. Resolving this has been difficult because rRNA-levels are hard to manipulate experimentally. Conventional approaches such as overexpression, knockdown, or knockout are ineffective owing to the high abundance of rRNA and the large number of rDNA genes. So far, indirect approaches have been necessary to manipulate rRNA-levels, such as inhibition of RNA Pol I (*25*), manipulation of its transcription factors (TFs) (*8*, *26*) or even broader regulators such as p53, PTEN, mTOR, or c-Myc (*27*, *28*). Although these approaches have provided important insights, they are not without ambiguity. Interference with RNA Pol I (e.g., via nucleostemin knockdown or the inhibitor CX-5461) induces cellular responses such as p53 activation and cell cycle arrest before detectable effects on rRNA synthesis, ribosome abundance, or translation (*25*, *29*, *30*). Moreover, supposedly specific RNA Pol I TFs (e.g., UBF) can also regulate RNA Pol II genes, (*31*); while general growth regulators like c-Myc or mTOR affect many additional pathways. Consequently, a direct method to induce rRNA transcription is needed to distinguish primary from secondary effects.

Here we developed a direct system for manipulating rRNA-levels by targeting CRISPR activators to the promoters of ribosomal transcripts (TAPIR, **T**argeted **A**ctivation of **P**rotein **T**ranslation).

**TAPIR induces transcriptional up-regulation of rRNA**

Since its introduction, CRISPR-based transactivation (CRISPRa) has been widely applied to RNA Pol II transcripts, mainly to induce protein-coding mRNAs and, to a lesser extent, long non-coding RNAs (*32*, *33*). To test whether RNA Pol I–dependent rRNAs can also be targeted, we designed gRNAs against the 47S precursor of 18S, 5.8S, and 28S rRNAs. Because rRNA genes cluster across chromosomes and contain repetitive elements in the mouse genome, individual gRNAs can target hundreds of regulatory sites (Fig. 1A). We generated neomycin-selectable plasmids expressing two gRNAs—one targeting a repetitive enhancer and one an upstream regulatory element (*34*–*38*)—using a published multiplexing strategy (*39*) and named it "r-gRNA1" (supplementary methods).

Because potent oncogenes such as c-Myc and KRAS, as well as immortalizing oncogenes, such as large T-antigen (LT) are known to strongly induce rRNA transcription (*40*–*42*), we reasoned that most commonly used cell lines might not be ideal to test experimental strategies of rRNA induction and its consequences. Instead we chose neural stem cells (NSCs) derived from the mouse forebrain (*43*). This provided the opportunity to test this approach in an accessible and meaningful in vitro system using highly developmentally relevant cells, which are neither derived from tumors nor deliberately immortalized. Moreover, it has been shown recently that, during prefrontal cortex specification, the number of ribosomes sharply decreases (Fig. 1B), indicating relevance of protein translation levels in this cell type (*44*). Additionally, NSCs proliferate rapidly in culture under self-renewing conditions (approximately one division every 24–36 hours), but are also able to readily exit the cell cycle and fully differentiate in vitro, when growth factors are removed from the culture medium (*45*), which enables studying the relevance of rRNA transcription in different cell identity contexts.

Compared to control gRNA-constructs, r-gRNA1 multiplied rRNA-levels two- to eleven-fold in NSCs when combined with a blasticidin-selectable CRISPR-based transactivation system (dCas9-VPR) (*46*), as measured by qPCR for 18S rRNA (Fig. 1C, white symbols). The magnitude of the effect came as a surprise, because even under physiological conditions rRNAs are estimated to account for a large majority of transcripts in mammalian cells (70-80%) (*2*). To exclude the possibility that detected effects might be dependent on antibiotic selection, we further revised our experimental strategy and equipped both, the dCas9-VPR and the gRNA-vectors with fluorescent-reporter-cassettes and repeated the experiment (Fig. 1C, black symbols). To ensure the effect would not be an artefact owing to a global down-regulation of mRNA, we quantified the mRNA-content of TAPIR-treated and control cells and confirmed that the poly-adenylated mRNA-content was not significantly different (fig. S1F and supplementary methods). To confirm the strong rRNA induction and to exclude that the detected effect was due to a PCR amplification-bias or normalization issue, we applied two more independent methods to quantify rRNA expression, high-resolution automated gel-electrophoresis and immunocytochemical analysis. High-resolution automated gel-electrophoresis confirmed that the absolute amount of rRNAs produced by a defined cell number (200,000 cells) was strongly induced after TAPIR and also indicated that elevated 45S transcripts were overall normally processed to transcripts that resemble 18S, 5.8S, and 28S rRNAs (Fig. 1D). Additionally, we included a second targeting vector, containing alternative gRNAs targeting 47S rDNA in this analysis (r-gRNA2; fig. S1, D and E). Immunocytochemistry applying the 5.8S rRNA–specific antibody Y10B confirmed the induction of rRNAs and indicated that induced rRNA species adopted the conformation necessary for antibody binding (Fig. 1, E to G).

To analyze, how CRISPR-mediated rDNA activation

affects the transcriptome, we applied RNA-Seq (Fig. 1H and fig. S2A). NSCs with and without TAPIR-treatment exhibited only subtle transcriptomic changes, because few genes (n=137) exhibited nominal differential expression ($p < 0.05$), with moderate effect sizes across samples. However, when genes were analyzed at the level of functional groups, treatment-associated changes became apparent. Among those was the up-regulation of a significant number of genes associated with rRNA transcription, processing and modification (Fig. 1H and supplementary methods). Taken together, this indicated that TAPIR was elevating rRNA transcription and a number of specific rRNA-associated genes.

NSCs are stem cells that have the potential to self-renew, but also to differentiate into terminally differentiated cells of the neural lineage, most efficiently (and often spontaneously) into astrocytes (*47*, *48*). To investigate, whether the observed activation of ribosomal RNA was dependent on a particular cellular state, we applied TAPIR and induced differentiation toward the astrocytic lineage through 4 day serum exposure. We also tested TAPIR in very fast cycling cells, the pluripotent mouse teratocarcinoma cell line P19, which can differentiate into cells of the three germ-layers, as well as primary mouse embryonic fibroblasts (MEFs) (fig. S1). Both the differentiating, as well as the pluripotent and primary cultures, responded with induction of rRNA, though less pronounced than in NSCs (Fig. 1, C to G, and fig. S1, A to C). This indicates that the approach is not strictly limited to the epigenetic landscape of somatic stem cells, but the chromatin context and basal expression levels of rRNA genes might influence its efficacy.

**TAPIR elevates protein translation levels**

Because three independent assays, one relying on the rRNA nucleotide sequence (qPCR), one on rRNA length (electrophoresis) and one on immunoreactivity to rRNA (Y10b staining), indicated that rRNA-levels were significantly elevated following CRISPR-mediated activation, we next investigated, how this might affect protein translation rates. To do this, we made use of O-Propargyl-puromycin incorporation and a click-iT reaction to measure nascent protein synthesis (*49*). The fluorescent reporter-cassettes enabled us to use flow cytometry to select for cells that receive and express both, dCas9- and gRNA-constructs (DsRed and eBFP), and to simultaneously measure protein translation in individual cells via detecting emission at 530/30nm (Fig. 2A).Cells that received r-gRNA-vectors exhibited elevated protein translation rates compared to controls. On average, cells generated between 35% to 60% more nascent polypeptides per hour than controls. Moreover, an induction of protein translation (12%-91%) was also detected when analyzing TAPIR treated fibroblast cultures (fig. S1, G and H).

As a next step, we performed ribosome profiling (ribo-seq) to assess the ribosome occupancy of mRNAs at a codon resolution. To this end we sorted 350,000 TAPIR-treated or control NSCs and performed low-input Ribo-Seq (Fig. 2B). Although sequencing depth was modest, quality control metrics were robust: the majority of mRNA reads mapped to coding regions (Fig. 2C), and clear P-site periodicity was observed (fig. S2, B and C). Global analysis of Ribo-Seq reads revealed that TAPIR treated cells exhibited an increased number of protein coding transcript reads compared to controls indicating higher ribosome occupancy and translational activity (Fig. 2D).

To characterize further which proteins were elevated in TAPIR-treated NSCs, we conducted proteome analysis by quantitative mass-spectrometry. We aimed to analyze whether elevated protein translation levels would result in a higher amount of protein per cell or whether this process would be compensated by other mechanisms (e.g., higher protein turnover). We were also interested whether all/most peptides would show elevated levels or instead a specific protein subset would be disproportionally induced, as seen during mid-neurogenesis (*44*). We exposed NSCs cultured in self-renewing conditions to TAPIR- or to control-constructs and 100,000 transfected cells were separated by FACS and analyzed 4 days later (N=6). Quantitative analysis of mass-spectrometry data using a high mass resolution quadrupole Orbitrap revealed that few proteins were strongly down-regulated (<0.75; n=7), which shared no meaningful function. In contrast, most were significantly increased in the TAPIR samples (>1.25; n=3833; 95.3%, $p < 0.013$, Welsh test). This clearly indicated a strong effect of rRNA induction on global cellular translation and steady state protein-levels (Fig. 2F). In good agreement with our previous results using O-Propargyl-puromycin-incorporation, the elevation averaged 1.56-fold that of the control samples indicating that induction of nascent protein translation is converted to higher cellular protein content overall. The induced proteins included all detected members of the large (40 of 43 proteins, 1.43-fold on average) and the small subunit of the ribosome (30 of 31 proteins, 1.48-fold on average). Proteins forming complexes necessary for rRNA procession and protein translation, including the exosome, a RNA exonuclease complex that is highly enriched in the nucleolus and necessary for 5.8S rRNA procession (*50*), were similarly elevated in the proteomic data. Eight of the ten exosome proteins conclusively detected were strongly induced after TAPIR (1.65-fold on average).

We also found a number of proteins with even higher induction (>3-fold; n=73). These included a number of proteins implicated in protein folding, such as Hgh1 and TTC4 (also called Cns1), both critical for maintaining translation elongation because they act as (co-)chaperones of the translation elongation factor eEF2 (*51*, *52*), as well as Ppic and Fkbp7 (*53*). In addition, several proteins with experimental evidence for

nucleolar location and/or ribosome function were part of this group, such as Naa25, a ribosomal anchor for the NatB complex (*54*). Other examples included the nucleolar WD repeat containing protein 74 (WDR74), involved in rRNA processing and the assembly of the large ribosomal subunit (*55*), Tnks1bp1 (*56*), and Ube2r2 (*57*). Rchy1, which is involved in the ribosome-associated quality control (RQC) pathway (*58*) and AK6 an essential gene regulating 18S rRNA processing and maturation of the small ribosomal subunit (*59*) also belonged to this group. Thus, TAPIR elevates both global protein translation levels and a specific signature.

**Elevation of rRNA transcription causes nucleoli expansion and cell cycle acceleration**

Because the proteomic analysis had revealed strong effects on a number of nucleolar factors, we next investigated the effect of TAPIR on the nucleoli structure. For this, we visualized nucleoli in NSCs exposed to TAPIR by immunostaining for Nucleolin, its major component, Fibrillarin, a frequently used marker of the dense fibrillary component, and the critical RNA Pol I TF, UBF1 (Fig. 3 and fig. S3). Although the number of Nucleolin or Fibrillarin structures per cell were not significantly affected (fig. S3, A and B), TAPIR changed the size of nucleoli. The effects for Fibrillarin and Nucleolin were evident in self-renewing NSCs. Here, elevation of rRNA level resulted in larger nucleoli, which is reflected by an elevated area per cell (Nucleolin p=0.0257; paired *t* test, Fibrillarin p=0.00487, paired *t* test), while the average nuclear area stayed unchanged (Fig. 3). UBF1 staining corroborated an increase in nucleolar area following TAPIR treatment (fig. S3C).

It has been suggested that nucleoli play a role in cellular proliferation (*60*). Because we also found an up-regulation of transcripts in the Gene Ontology "Whitfield_cell_cycle_G1/S," category (NES=-2.1, pval=9.1*10^-6; Fig. 1H) in our transcriptome analysis of TAPIR-treated cells, we next investigated the effect of 47S rDNA activation on cellular growth rates. For this, we analyzed proliferation markers by immunostaining after 4 days and measured cell number after a further 4 days. NSCs cultured in self-renewal conditions are fast growing cells with an estimated doubling-time of ca 29h, comprising many $K_i$-67 (marking proliferation), proliferating cell nuclear antigen (PCNA, indicating an active cell cycle) and phospho-histone 3 (PH3) positive cells (labeling mitotic cells and late G2; Fig. 4B). TAPIR treated cells significantly increased the proportion of PCNA- (Ctrl: 18.9% ± 5.4%, TAPIR: 30.9% ± 4% n=3) and PH3-positive cells (Ctrl: 10.7% ± 4.7%, TAPIR: 18.6% ± 3.5%, n=4).Three days later the number of mitotic cells reverted back to normal levels, likely due to a dilution of the transiently transfected CRISPR tools (Fig. 4, B to E). Nevertheless, the relative cell number compared to control cells had doubled during this time (Fig. 4A). This suggests that TAPIR treated NSCs shorten their doubling time by at least ~25%, almost matching that of NIH-3T3 cells (~22h). This effect was observed under self-renewing conditions and during glial differentiation. While most control cells had left an active cell cycle 4d after induction of differentiation, the number of mitotic figures were as frequent in TAPIR treated differentiating NSCs as during self-renewing conditions (Fig. 4, B to E) and only reverted to control levels at d10.

**Elevated protein translation rates enhance self-renewal of NSCs in vitro**

Next, we investigated how protein translation levels might affect the fates of NSCs. Immunoblot analysis (fig. S4) did not show a significant increase of key signaling pathway proteins (mTOR1, N-MYC, STAT1, STAT3, JAK, AKT1, p70) or modifications (p-AKT1, p-STAT1, p-STAT3) implicated in cellular growth relative to a housekeeper gene (β-Actin). Neither did we detect any elevation of the initiator protease of the intrinsic apoptotic pathway (Caspase 9). This is in line with the transcriptome analysis showing no significant enrichment for GO-pathways such as "Apoptosis" or the "Unfolded_Protein_Response_(UPR)" (Fig. 1H). In contrast, we found a widespread depletion of transcripts associated with astrocyte signatures (LEIN_astrocyte_markers: NES=-1.81, pval=0.014; GOBP_astrocyte_development: NES=-1.83, pval=0.013), indicating reduced spontaneous stem cell differentiation. To confirm this finding, we made use of four neural identity markers in particular: Sox2, a critical stem cell factor, and Nestin, a stem cell marker, labeling a majority of NSCs under self-renewal conditions (79.5% ± 4.3%, n=7 and 89.0% ± 0.5% d, n=4 respectively, fig. S5A), but were mostly absent after cellular differentiation. TAPIR increased the proportion of Sox2-positive and Nestin-positive NSCs cells during self-renewal conditions significantly to 89.5% ±3.8% (paired T-Test, p<0.05) and to 93.7%±0.3% (paired T-Test, p<0.003) respectively (fig. S5A). After 4 days in differentiation media, most control cells underwent extensive morphological changes and expressed GFAP, a widely used marker of astrocytic differentiation, and S100b, a more mature astrocyte marker, (73.3% ± 3.6%, n=7 and 82.2% ± 1.7% d, n=4, respectively) (fig. S5B). TAPIR however significantly decreased GFAP and S100b immuno-reactivity during differentiation (57.1%± 4.8%, paired T-Test, p<0.005 and 69.5%± 3.3%, paired T-Test, p<0.02).

**Elevated rRNA transcription enhances self-renewal of NSCs in vivo**

Because these data indicated that TAPIR elevates self-renewal of NSCs in vitro, we next investigated, whether a similar effect would be triggered in vivo. For this, we employed in utero electroporation of TAPIR into one lateral ventricle of the forebrain of embryonic day 13.5 (E13.5) embryos, as previously (*61*, *62*). 48hrs later, we removed, fixed and sectioned

the brains and analyzed the position and identity of double electroporated cells via immunohistochemistry (Fig. 5A). Non-electroporated (as well as control electroporated) hemispheres were characterized by two defined bands of mitotic cells (labeled by PH3): One lies directly at the ventricular surface made up of the Pax6-expressing NSCs of the forebrain, the apical radial glia cells (aRGC); while the other band is defined by Tbr2-positive basal progenitors (*63*). TAPIR electroporated cortices exhibited many more mitotic cells among the double electroporated cells that were also more widespread compared to controls (Fig. 5, B to D, and fig. S6). This indicated that 47S rDNA induction and elevation of protein translation promoted an active cell cycle in somatic NSCs in vivo. Analysis of animals at a later timepoint (P10) using a single PiggyBAC-construct (expressing both dCas9-VPR and rRNA1) revealed that many TAPIR-positive cells survived and frequently differentiated into NeuN-positive neurons (fig. S6E). Although at E15.5 PH3-positive cells were elevated throughout most of the cortex (bin 1-4), they were significantly enriched at the natural mitotic niches (SVZ and intermediate zone; Fig. 5, B to D). Moreover, a significant increase in cells positive for the aRGC marker Pax6 was detected in bin 3, consisting of mostly Pax6-negative cells in the controls (fig. S6, A to C). These results demonstrate that the effects of rRNA induction and cellular protein translation rates on NSC expansion were not limited to cells cultured in metabolically optimal conditions, but similar effects on cellular growth could be triggered during organ development in vivo.

**TAPIR enables modeling and attenuation of disease phenotypes**

To test whether targeted rRNA induction could be used to model or treat human diseases, we applied TAPIR to mouse models of two human diseases, ribosomopathy and cancer. Given that targeted activation of rRNA transcription markedly promoted cell cycle progression, we investigated first whether it recapitulates hallmark features of cancer. For this, we made use of an established mouse model of pancreatic ductal adenocarcinoma (PDAC) based on inducible expression of oncogenic KRAS (*64*). Cells derived from these mice show many hallmarks of cancer cells, including uncontrolled proliferation and survival under non-adherent conditions, features that can be quantified in colony assays in vitro. PDAC cells also showed high levels of rRNAs (*42*), quantifiable through a strong accumulation of nascent RNA in the nucleolus, visualized by pulse-labeling with Fluorouridine (FUrd) and immunocytochemistry with an antibody against FUrd (Fig. 6A and supplementary methods) (*65*). High levels of nascent rRNAs were dependent on continuous expression of oncogenic KRAS, and could be blocked by treatment with CX-5461 (*42*) (Fig. 6B). Similarly, colony formation and growth of the cells was boosted by KRAS, but could be inhibited by CX-5461. TAPIR could replace oncogenic KRAS for rRNA activation (Fig. 6, A and B) and promoted growth of PDAC cells in colony formation assays (Fig. 6, C and D). This indicates a key role for enhancement of rRNA synthesis in oncogene-induced growth. Furthermore, the lack of additive effects suggests that cancer cell lines may exhibit limited sensitivity to TAPIR owing to the already strong levels of oncogene-induced rRNA expression (Fig. 6C).

**TAPIR attenuates cellular phenotypes associated with ribosomopathies**

Ribosomopathies are a group of human disorders caused by defects in ribosome biogenesis or function. They usually manifest as developmental abnormalities, often caused by p53-dependent apoptosis (*22*). To investigate whether TAPIR could ameliorate the effects of disease causing mutations, we made use of an established mouse model of Treacher Collins syndrome, a classic ribosomopathy disorder. Treacher Collins syndrome is primarily associated with variants in *TCOF1*, which together with RNA Pol I drive rDNA transcription. Haploinsufficiency of *Tcof1* in mice results in diminished rRNA level and decreased protein translation (*66*). MEFs were derived from E13.5 and E14.5 *Tcof1flx/flx;Cre-ERT2* embryos, generated by crossing *Tcof1*$^{flx/flx}$ mice to tamoxifen-inducible *Cre-ERT2* mice (*22*). Compared to untreated MEFs, deletion of Tcof1/Treacle resulted in gross morphological changes and decreased cell number (Fig. 6E and fig. S5C). TAPIR treatment reduced these effects with cell morphology and number normalized. Thus, TAPIR or a similar strategy could be useful to ameliorate the developmental effects observed in ribosomopathies.

**A strategy for TAPIR in human cells**

To be applicable to address human diseases, we next aimed to establish a TAPIR strategy for human cells. We have established TAPIR for mouse rDNA, which contains repetitive sequence modules containing PAM sequences (Fig. 1A). Human rDNA loci however lack a repetitive structure, making high-density binding of transactivators difficult. To nevertheless establish TAPIR in human cells, we developed a CRISPRa strategy based on direct delivery of dCas9-VPR protein (dRNPs), thereby reducing constraints associated with multiplexed gRNA numbers (*67*). Applying dRNPs with 14 gRNAs targeting the human rDNA promoter resulted in a significant induction of rRNA expression (Fig. 6, F and G) and nascent protein translation (fig. S7) in a human T cell line, although at lower levels compared to mouse.

**Discussion**

Research on regulators of stem cells mostly focuses on factors and mechanisms with specificity, such as TF networks, signaling pathways and epigenetic features (*68*). Known factors

regulating corticogenesis include the TF Pax6 (*69*), Shh signaling (*70*) and DNA de-methylation (*71*). Here we identify an additional mechanism. Recent reports have hinted already at the critical importance of "house-keeping" processes (*72*) and ribosome biogenesis for cell type identity (*1*, *73*). Moreover, it has been reported that facultative translation initiation factors govern neuronal output of aRGCs (*44*), while the nucleolar protein Trnp1 regulates cortical thickness (*61*). However, whether rRNA expression has direct regulatory functions and how global protein translation-level influence cell behavior remained elusive until now.

TAPIR increased NSC expansion in vitro and in the developing mouse forebrain in vivo. Moreover, the finding that the apical radial glia factor Pax6 is detected after TAPIR in regions occupied by basal progenitors suggests an expansion of basal radial glia cells, as seen in gyrencephalic species like humans, or a possible fate reversion of basal progenitors to NSCs. Comparable links between ribosome abundance and cell fate decisions have recently been reported in hematopoiesis (*23*) and during T-cell activation (*74*). TAPIR itself is clearly modulated by developmental cues: cells exposed to strong differentiation signals ultimately overcame the induced differentiation block, both in vitro and at later stages in vivo (P10). However, this does not necessarily indicate that rRNA lacks phenotypic sufficiency. Rather, it may reflect reduced efficacy of TAPIR in differentiating cells. Additional regulatory mechanisms, such as DNA methylation, may contribute to this context-dependent modulation and could represent potential targets to enhance the effectiveness of TAPIR.

The observation that following TAPIR multiple nucleolar proteins are induced significantly higher than the observed proteome-wide increase indicates a cellular response program downstream of rRNA transcription. This consequently points toward a regulatory function of rRNA-levels in physiological (e.g., embryonic development) and pathological conditions (e.g., cancer). In agreement with our results, it has been shown in Drosophila that overexpression of a Polymerase I regulatory protein TiF1α (*26*) can lead to an increase in cellular proliferation in the germ line. Targeted approaches to manipulate rRNA-levels directly, such as TAPIR will be instrumental to investigate, how widespread stem cell regulation by global protein translation levels is. Considering the high rRNA-level in pluripotent stem cells (*73*, *75*) and the particularly low protein translation-level in quiescent stem cells (*76*), it seems probable that this mechanism might be of general relevance.

TAPIR employs a composite fusion protein, dCas9-VPR, containing three transactivator domains of RNA Pol II TFs: VP64, p65 and RTA (*46*). These TFs have to our knowledge not yet been implicated in regulation of RNA Pol I. Due to the observed TAPIR induced increase of 47S and functional 18S and 28S rRNAs, we suspect that those protein domains have transactivating effects beyond RNA Pol II and that elevated rRNA-levels can be attributed to increased RNA Pol I binding or activity at the rDNA genes. This is in line with the efficacy of the inhibitor CX-5461 on TAPIR treated cells. We found that TAPIR increases nucleoli size indicating that previously repressed or stably silenced rDNA genes might be responsible for the elevated rRNA-levels. The fact that the nucleolar changes were, however, relative small compared to the transcriptional increase suggests as well, that a larger proportion is derived from already open and/or poised rDNA genes (*77*). We also show that the effectiveness of TAPIR is limited by the genetic makeup of the target cells. We provide evidence that potent oncogenes, such as oncogenic KRAS, mirror TAPIR's effect and saturate nascent rRNA level. This might explain, why the efficacy of TAPIR on cancer and immortalized cell lines might be lower in general. Moreover, species differences in the rDNA promoter limit trans-activator binding. Nevertheless, novel CRISPR tools (such as dRNPs), can overcome this hurdle.

TAPIR offers a unique option for targeted manipulation of 47S rRNA expression, which is of highest relevance for studying regulation of protein translation under physiological conditions and in a large number of disease (*2*, *13*). Not only does TAPIR provide a first strategic tool to potentially treat ribosomopathies, diseases that are caused directly by the loss of one component of the protein translation machinery or the reduction of rRNA (*78*), such as Treacher-Collins-syndrome and Diamond-Blackfan anemia (*79*), but similar approaches could also be applied to those conditions in which rRNA misregulation has been reported, such as cancer (*12*), neurodegenerative diseases (*16*) and aging (*20*, *21*).

Materials and methods are available in the supplementary materials.

## REFERENCES AND NOTES


1. J. A. Saba, K. Liakath-Ali, R. Green, F. M. Watt, Translational control of stem cell function. *Nat. Rev. Mol. Cell Biol.* **22**, 671–690 (2021). doi:10.1038/s41580-021-00386-2 Medline
2. J. Diesch, R. D. Hannan, E. Sanij, Perturbations at the ribosomal genes loci are at the centre of cellular dysfunction and human disease. *Cell Biosci.* **4**, 43 (2014). doi:10.1186/2045-3701-4-43 Medline
3. J. G. Gibbons, A. T. Branco, S. A. Godinho, S. Yu, B. Lemos, Concerted copy number variation balances ribosomal DNA dosage in human and mouse genomes. *Proc. Natl. Acad. Sci. U.S.A.* **112**, 2485–2490 (2015). doi:10.1073/pnas.1416878112 Medline
4. A. K. Henras, C. Plisson-Chastang, M. F. O'Donohue, A. Chakraborty, P. E. Gleizes, An overview of pre-ribosomal RNA processing in eukaryotes. *Wiley Interdiscip. Rev. RNA* **6**, 225–242 (2015). doi:10.1002/wrna.1269 Medline
5. F. Pontvianne, T. Blevins, C. Chandrasekhara, I. Mozgová, C. Hassel, O. M. F. Pontes, S. Tucker, P. Mokroš, V. Muchová, J. Fajkus, C. S. Pikaard, Subnuclear partitioning of rRNA genes between the nucleolus and nucleoplasm reflects alternative epiallelic states. *Genes Dev.* **27**, 1545–1550 (2013). doi:10.1101/gad.221648.113 Medline
6. Y. Hori, C. Engel, T. Kobayashi, Regulation of ribosomal RNA gene copy number, transcription and nucleolus organization in eukaryotes. *Nat. Rev. Mol. Cell Biol.* **24**, 414–429 (2023). doi:10.1038/s41580-022-00573-9 Medline

7. S. Sharifi, H. F. R. da Costa, H. Bierhoff, The circuitry between ribosome biogenesis and translation in stem cell function and ageing. *Mech. Ageing Dev.* **189**, 111282 (2020). doi:10.1016/j.mad.2020.111282 Medline
8. S. A. Ali, S. K. Zaidi, C. S. Dacwag, N. Salma, D. W. Young, A. R. Shakoori, M. A. Montecino, J. B. Lian, A. J. van Wijnen, A. N. Imbalzano, G. S. Stein, J. L. Stein, Phenotypic transcription factors epigenetically mediate cell growth control. *Proc. Natl. Acad. Sci. U.S.A.* **105**, 6632–6637 (2008). doi:10.1073/pnas.0800970105 Medline
9. Y. Hayashi, T. Kuroda, H. Kishimoto, C. Wang, A. Iwama, K. Kimura, Downregulation of rRNA transcription triggers cell differentiation. *PLOS ONE* **9**, e98586 (2014). doi:10.1371/journal.pone.0098586 Medline
10. M. Buszczak, R. A. Signer, S. J. Morrison, Cellular differences in protein synthesis regulate tissue homeostasis. *Cell* **159**, 242–251 (2014). doi:10.1016/j.cell.2014.09.016 Medline
11. M. Cook, M. Tyers, Size control goes global. *Curr. Opin. Biotechnol.* **18**, 341–350 (2007). doi:10.1016/j.copbio.2007.07.006 Medline
12. M. J. Bywater, R. B. Pearson, G. A. McArthur, R. D. Hannan, Dysregulation of the basal RNA polymerase transcription apparatus in cancer. *Nat. Rev. Cancer* **13**, 299–314 (2013). doi:10.1038/nrc3496 Medline
13. L. X. T. Nguyen, A. Raval, J. S. Garcia, B. S. Mitchell, Regulation of ribosomal gene expression in cancer. *J. Cell. Physiol.* **230**, 1181–1188 (2015). doi:10.1002/jcp.24854 Medline
14. I. B. Rosenwald, The role of translation in neoplastic transformation from a pathologist's point of view. *Oncogene* **23**, 3230–3247 (2004). doi:10.1038/sj.onc.1207552 Medline
15. C. Morral, J. Stanisavljevic, X. Hernando-Momblona, E. Mereu, A. Álvarez-Varela, C. Cortina, D. Stork, F. Slebe, G. Turon, G. Whissell, M. Sevillano, A. Merlos-Suárez, À. Casanova-Martí, C. Moutinho, S. W. Lowe, L. E. Dow, A. Villanueva, E. Sancho, H. Heyn, E. Batlle, Zonation of ribosomal DNA transcription defines a stem cell hierarchy in colorectal cancer. *Cell Stem Cell* **26**, 845–861.e12 (2020). doi:10.1016/j.stem.2020.04.012 Medline
16. R. Parlato, B. Liss, How Parkinson's disease meets nucleolar stress. *Biochim. Biophys. Acta* **1842**, 791–797 (2014). doi:10.1016/j.bbadis.2013.12.014 Medline
17. J. A. Moreno, H. Radford, D. Peretti, J. R. Steinert, N. Verity, M. G. Martin, M. Halliday, J. Morgan, D. Dinsdale, C. A. Ortori, D. A. Barrett, P. Tsaytler, A. Bertolotti, A. E. Willis, M. Bushell, G. R. Mallucci, Sustained translational repression by eIF2$\alpha$-P mediates prion neurodegeneration. *Nature* **485**, 507–511 (2012). doi:10.1038/nature11058 Medline
18. M. S. LeDoux, Polymerase I as a target for treating neurodegenerative disorders. *Biomedicines* **12**, 1092 (2024). doi:10.3390/biomedicines12051092 Medline
19. C. Ni, Y. Wei, B. Vona, D. Park, Y. Wei, D. A. Schmitz, Y. Ding, M. Sakurai, E. Ballard, L. Li, Y. Liu, A. Kumar, C. Xing, S. Qin, S. Kim, M. Foglizzo, J. Zhao, H.-G. Kim, C. Ekmekci, E. G. Karimiani, S. Imannezhad, F. Eghbal, R. S. Badv, E. M. C. Schwaibold, M. Dehghani, M. Y. V. Mehrjardi, Z. Metanat, H. Eslamiyeh, E. Khouj, S. M. N. Alhajj, A. Chedrawi, K. Ramzan, J. A. Hashmi, M. M. Alluqmani, S. Basit, D. Veltra, N. M. Marinakis, G. Niotakis, P. Vorgia, C. Sofocleous, H. Lee, W. C. Jeong, M. Umair, M. Bilal, C. A. P. F. Alves, M. Sieber, M. Kruer, H. Houlden, F. S. Alkuraya, E. Zeqiraj, R. A. Greenberg, C. Cenik, L. Yu, R. Maroofian, J. Wu, M. Buszczak, A programmed decline in ribosome levels governs human early neurodevelopment. *Nat. Cell Biol.* **27**, 1240–1255 (2025). doi:10.1038/s41556-025-01708-8 Medline
20. K. K. Steffen, A. Dillin, A ribosomal perspective on proteostasis and aging. *Cell Metab.* **23**, 1004–1012 (2016). doi:10.1016/j.cmet.2016.05.013 Medline
21. L. M. García Moreno, J. M. Cimadevilla, H. González Pardo, M. C. Zahonero, J. L. Arias, NOR activity in hippocampal areas during the postnatal development and ageing. *Mech. Ageing Dev.* **97**, 173–181 (1997). doi:10.1016/S0047-6374(97)00054-7 Medline
22. K. T. Falcon, K. E. N. Watt, S. Dash, R. Zhao, D. Sakai, E. L. Moore, S. Fitriasari, M. Childers, M. E. Sardiu, S. Swanson, D. Tsuchiya, J. Unruh, G. Bugarinovic, L. Li, R. Shiang, A. Achilleos, J. Dixon, M. J. Dixon, P. A. Trainor, Dynamic regulation and requirement for ribosomal RNA transcription during mammalian development. *Proc. Natl. Acad. Sci. U.S.A.* **119**, e2116974119 (2022). doi:10.1073/pnas.2116974119 Medline
23. R. K. Khajuria, M. Munschauer, J. C. Ulirsch, C. Fiorini, L. S. Ludwig, S. K. McFarland, N. J. Abdulhay, H. Specht, H. Keshishian, D. R. Mani, M. Jovanovic, S. R. Ellis, C. P. Fulco, J. M. Engreitz, S. Schütz, J. Lian, K. W. Gripp, O. K. Weinberg, G. S. Pinkus, L. Gehrke, A. Regev, E. S. Lander, H. T. Gazda, W. Y. Lee, V. G. Panse, S. A. Carr, V. G. Sankaran, Ribosome levels selectively regulate translation and lineage commitment in human hematopoiesis. *Cell* **173**, 90–103.e19 (2018). doi:10.1016/j.cell.2018.02.036 Medline
24. P. A. Trainor, A. E. Merrill, Ribosome biogenesis in skeletal development and the pathogenesis of skeletal disorders. *Biochim. Biophys. Acta* **1842**, 769–778 (2014). doi:10.1016/j.bbadis.2013.11.010 Medline
25. M. J. Bywater, G. Poortinga, E. Sanij, N. Hein, A. Peck, C. Cullinane, M. Wall, L. Cluse, D. Drygin, K. Anderes, N. Huser, C. Proffitt, J. Bliesath, M. Haddach, M. K. Schwaebe, D. M. Ryckman, W. G. Rice, C. Schmitt, S. W. Lowe, R. W. Johnstone, R. B. Pearson, G. A. McArthur, R. D. Hannan, Inhibition of RNA polymerase I as a therapeutic strategy to promote cancer-specific activation of p53. *Cancer Cell* **22**, 51–65 (2012). doi:10.1016/j.ccr.2012.05.019 Medline
26. Q. Zhang, N. A. Shalaby, M. Buszczak, Changes in rRNA transcription influence proliferation and cell fate within a stem cell lineage. *Science* **343**, 298–301 (2014). doi:10.1126/science.1246384 Medline
27. S. Sharifi, H. Bierhoff, Regulation of RNA polymerase I transcription in development, disease, and aging. *Annu. Rev. Biochem.* **87**, 51–73 (2018). doi:10.1146/annurev-biochem-062917-012612 Medline
28. L. Hua, D. Yan, C. Wan, B. Hu, Nucleolus and nucleolar stress: From cell fate decision to disease development. *Cells* **11**, 3017 (2022). doi:10.3390/cells11193017 Medline
29. R. Y. Tsai, T. Pederson, Connecting the nucleolus to the cell cycle and human disease. *FASEB J.* **28**, 3290–3296 (2014). doi:10.1096/fj.14-254680 Medline
30. T. Lin, L. Meng, T. C. Lin, L. J. Wu, T. Pederson, R. Y. Tsai, Nucleostemin and GNL3L exercise distinct functions in genome protection and ribosome synthesis, respectively. *J. Cell Sci.* **127**, 2302–2312 (2014). doi:10.1242/jcs.143842 Medline
31. E. Sanij, J. Diesch, A. Lesmana, G. Poortinga, N. Hein, G. Lidgerwood, D. P. Cameron, J. Ellul, G. J. Goodall, L. H. Wong, A. S. Dhillon, N. Hamdane, L. I. Rothblum, R. B. Pearson, I. Haviv, T. Moss, R. D. Hannan, A novel role for the Pol I transcription factor UBTF in maintaining genome stability through the regulation of highly transcribed Pol II genes. *Genome Res.* **25**, 201–212 (2015). doi:10.1101/gr.176115.114 Medline
32. J. Joung, J. M. Engreitz, S. Konermann, O. O. Abudayyeh, V. K. Verdine, F. Aguet, J. S. Gootenberg, N. E. Sanjana, J. B. Wright, C. P. Fulco, Y.-Y. Tseng, C. H. Yoon, J. S. Boehm, E. S. Lander, F. Zhang, Genome-scale activation screen identifies a lncRNA locus regulating a gene neighbourhood. *Nature* **548**, 343–346 (2017). doi:10.1038/nature23451 Medline
33. C. T. Breunig, A. Köferle, A. M. Neuner, M. F. Wiesbeck, V. Baumann, S. H. Stricker, CRISPR tools for physiology and cell state changes: Potential of transcriptional engineering and epigenome editing. *Physiol. Rev.* **101**, 177–211 (2021). doi:10.1152/physrev.00034.2019 Medline
34. R. F. De Winter, T. Moss, Spacer promoters are essential for efficient enhancement of X. laevis ribosomal transcription. *Cell* **44**, 313–318 (1986). doi:10.1016/0092-8674(86)90765-8 Medline
35. G. Grimaldi, P. Fiorentini, P. P. Di Nocera, Spacer promoters are orientation-dependent activators of pre-rRNA transcription in *Drosophila melanogaster*. *Mol. Cell. Biol.* **10**, 4667–4677 (1990). doi:10.1128/mcb.10.9.4667-4677.1990 Medline
36. J. R. Miller, D. C. Hayward, D. M. Glover, Transcription of the 'non-transcribed' spacer of *Drosophila melanogaster* rDNA. *Nucleic Acids Res.* **11**, 11–19 (1983). doi:10.1093/nar/11.1.11 Medline
37. T. Moss, A transcriptional function for the repetitive ribosomal spacer in *Xenopus laevis*. *Nature* **302**, 223–228 (1983). doi:10.1038/302223a0 Medline
38. A. A. Caudy, C. S. Pikaard, Xenopus ribosomal RNA gene intergenic spacer elements conferring transcriptional enhancement and nucleolar dominance-like competition in oocytes. *J. Biol. Chem.* **277**, 31577–31584 (2002). doi:10.1074/jbc.M202737200 Medline
39. C. T. Breunig, T. Durovic, A. M. Neuner, V. Baumann, M. F. Wiesbeck, A. Köferle, M. Götz, J. Ninkovic, S. H. Stricker, One step generation of customizable gRNA vectors for multiplex CRISPR approaches through string assembly gRNA cloning (STAgR). *PLOS ONE* **13**, e0196015 (2018). doi:10.1371/journal.pone.0196015 Medline
40. W. Zhai, J. A. Tuan, L. Comai, SV40 large T antigen binds to the TBP-TAF(I) complex SL1 and coactivates ribosomal RNA transcription. *Genes Dev.* **11**, 1605–1617 (1997). doi:10.1101/gad.11.12.1605 Medline

41. C. Grandori, N. Gomez-Roman, Z. A. Felton-Edkins, C. Ngouenet, D. A. Galloway, R. N. Eisenman, R. J. White, c-Myc binds to human ribosomal DNA and stimulates transcription of rRNA genes by RNA polymerase I. *Nat. Cell Biol.* **7**, 311–318 (2005). doi:10.1038/ncb1224 Medline
42. M. S. Azman, E. L. Alard, M. Dodel, F. Capraro, R. Faraway, M. Dermit, W. Fan, A. Chakraborty, J. Ule, F. K. Mardakheh, An ERK1/2-driven RNA-binding switch in nucleolin drives ribosome biogenesis and pancreatic tumorigenesis downstream of RAS oncogene. *EMBO J.* **42**, e110902 (2023). doi:10.15252/embj.2022110902 Medline
43. L. Conti, S. M. Pollard, T. Gorba, E. Reitano, M. Toselli, G. Biella, Y. Sun, S. Sanzone, Q.-L. Ying, E. Cattaneo, A. Smith, Niche-independent symmetrical self-renewal of a mammalian tissue stem cell. *PLOS Biol.* **3**, e283 (2005). doi:10.1371/journal.pbio.0030283 Medline
44. D. Harnett, M. C. Ambrozkiewicz, U. Zinnall, A. Rusanova, E. Borisova, A. N. Drescher, M. Couce-Iglesias, G. Villamil, R. Dannenberg, K. Imami, A. Münster-Wandowski, B. Fauler, T. Mielke, M. Selbach, M. Landthaler, C. M. T. Spahn, V. Tarabykin, U. Ohler, M. L. Kraushar, A critical period of translational control during brain development at codon resolution. *Nat. Struct. Mol. Biol.* **29**, 1277–1290 (2022). doi:10.1038/s41594-022-00882-9 Medline
45. S. Gómez-López, O. Wiskow, R. Favaro, S. K. Nicolis, D. J. Price, S. M. Pollard, A. Smith, Sox2 and Pax6 maintain the proliferative and developmental potential of gliogenic neural stem cells *In vitro*. *Glia* **59**, 1588–1599 (2011). doi:10.1002/glia.21201 Medline
46. A. Chavez, J. Scheiman, S. Vora, B. W. Pruitt, M. Tuttle, E. P R Iyer, S. Lin, S. Kiani, C. D. Guzman, D. J. Wiegand, D. Ter-Ovanesyan, J. L. Braff, N. Davidsohn, B. E. Housden, N. Perrimon, R. Weiss, J. Aach, J. J. Collins, G. M. Church, Highly efficient Cas9-mediated transcriptional programming. *Nat. Methods* **12**, 326–328 (2015). doi:10.1038/nmeth.3312 Medline
47. S. M. Pollard, L. Conti, Y. Sun, D. Goffredo, A. Smith, Adherent neural stem (NS) cells from fetal and adult forebrain. *Cereb. Cortex* **16** (suppl. 1), i112–i120 (2006). doi:10.1093/cercor/bhj167 Medline
48. V. Baumann, M. Wiesbeck, C. T. Breunig, J. M. Braun, A. Köferle, J. Ninkovic, M. Götz, S. H. Stricker, Targeted removal of epigenetic barriers during transcriptional reprogramming. *Nat. Commun.* **10**, 2119 (2019). doi:10.1038/s41467-019-10146-8 Medline
49. J. Liu, Y. Xu, D. Stoleru, A. Salic, Imaging protein synthesis in cells and tissues with an alkyne analog of puromycin. *Proc. Natl. Acad. Sci. U.S.A.* **109**, 413–418 (2012). doi:10.1073/pnas.1111561108 Medline
50. C. Allmang, J. Kufel, G. Chanfreau, P. Mitchell, E. Petfalski, D. Tollervey, Functions of the exosome in rRNA, snoRNA and snRNA synthesis. *EMBO J.* **18**, 5399–5410 (1999). doi:10.1093/emboj/18.19.5399 Medline
51. F. H. Schopf, E. M. Huber, C. Dodt, A. Lopez, M. M. Biebl, D. A. Rutz, M. Mühlhofer, G. Richter, T. Madl, M. Sattler, M. Groll, J. Buchner, The co-chaperone Cns1 and the recruiter protein Hgh1 link Hsp90 to translation elongation via chaperoning elongation factor 2. *Mol. Cell* **74**, 73–87.e8 (2019). doi:10.1016/j.molcel.2019.02.011 Medline
52. L. Mönkemeyer, C. L. Klaips, D. Balchin, R. Körner, F. U. Hartl, A. Bracher, Chaperone function of Hgh1 in the biogenesis of eukaryotic elongation factor 2. *Mol. Cell* **74**, 88–100.e9 (2019). doi:10.1016/j.molcel.2019.01.034 Medline
53. F. U. Hartl, M. Hayer-Hartl, Converging concepts of protein folding *in vitro* and *in vivo*. *Nat. Struct. Mol. Biol.* **16**, 574–581 (2009). doi:10.1038/nsmb.1591 Medline
54. R. Ree, S. Varland, T. Arnesen, Spotlight on protein N-terminal acetylation. *Exp. Mol. Med.* **50**, 1–13 (2018). doi:10.1038/s12276-018-0116-z Medline
55. N. Hiraishi, Y. Ishida, M. Nagahama, AAA-ATPase NVL2 acts on MTR4-exosome complex to dissociate the nucleolar protein WDR74. *Biochem. Biophys. Res. Commun.* **467**, 534–540 (2015). doi:10.1016/j.bbrc.2015.09.160 Medline
56. H. Seimiya, S. Smith, The telomeric poly(ADP-ribose) polymerase, tankyrase 1, contains multiple binding sites for telomeric repeat binding factor 1 (TRF1) and a novel acceptor, 182-kDa tankyrase-binding protein (TAB182). *J. Biol. Chem.* **277**, 14116–14126 (2002). doi:10.1074/jbc.M112266200 Medline
57. M. Uhlén, L. Fagerberg, B. M. Hallström, C. Lindskog, P. Oksvold, A. Mardinoglu, Å. Sivertsson, C. Kampf, E. Sjöstedt, A. Asplund, I. Olsson, K. Edlund, E. Lundberg, S. Navani, C. A.-K. Szigyarto, J. Odeberg, D. Djureinovic, J. O. Takanen, S. Hober, T. Alm, P.-H. Edqvist, H. Berling, H. Tegel, J. Mulder, J. Rockberg, P. Nilsson, J. M. Schwenk, M. Hamsten, K. von Feilitzen, M. Forsberg, L. Persson, F. Johansson, M. Zwahlen, G. von Heijne, J. Nielsen, F. Pontén, Tissue-based map of the human proteome. *Science* **347**, 1260419 (2015). doi:10.1126/science.1260419 Medline
58. A. Thrun, A. Garzia, Y. Kigoshi-Tansho, P. R. Patil, C. S. Umbaugh, T. Dallinger, J. Liu, S. Kreger, A. Patrizi, G. A. Cox, T. Tuschl, C. A. P. Joazeiro, Convergence of mammalian RQC and C-end rule proteolytic pathways via alanine tailing. *Mol. Cell* **81**, 2112–2122.e7 (2021). doi:10.1016/j.molcel.2021.03.004 Medline
59. D. Bai, J. Zhang, T. Li, R. Hang, Y. Liu, Y. Tian, D. Huang, L. Qu, X. Cao, J. Ji, X. Zheng, The ATPase hCINAP regulates 18S rRNA processing and is essential for embryogenesis and tumour growth. *Nat. Commun.* **7**, 12310 (2016). doi:10.1038/ncomms12310 Medline
60. F. M. Boisvert, S. van Koningsbruggen, J. Navascués, A. I. Lamond, The multifunctional nucleolus. *Nat. Rev. Mol. Cell Biol.* **8**, 574–585 (2007). doi:10.1038/nrm2184 Medline
61. R. Stahl, T. Walcher, C. De Juan Romero, G. A. Pilz, S. Cappello, M. Irmler, J. M. Sanz-Aquela, J. Beckers, R. Blum, V. Borrell, M. Götz, Trnp1 regulates expansion and folding of the mammalian cerebral cortex by control of radial glial fate. *Cell* **153**, 535–549 (2013). doi:10.1016/j.cell.2013.03.027 Medline
62. A. C. O'Neill, F. Uzbas, G. Antognolli, F. Merino, K. Draganova, A. Jäck, S. Zhang, G. Pedini, J. P. Schessner, K. Cramer, A. Schepers, F. Metzger, M. Esgleas, P. Smialowski, R. Guerrini, S. Falk, R. Feederle, S. Freytag, Z. Wang, M. Bahlo, R. Jungmann, C. Bagni, G. H. H. Borner, S. P. Robertson, S. M. Hauck, M. Götz, Spatial centrosome proteome of human neural cells uncovers disease-relevant heterogeneity. *Science* **376**, eabf9088 (2022). doi:10.1126/science.abf9088 Medline
63. M. Götz, W. B. Huttner, The cell biology of neurogenesis. *Nat. Rev. Mol. Cell Biol.* **6**, 777–788 (2005). doi:10.1038/nrm1739 Medline
64. H. Ying, A. C. Kimmelman, C. A. Lyssiotis, S. Hua, G. C. Chu, E. Fletcher-Sananikone, J. W. Locasale, J. Son, H. Zhang, J. L. Coloff, H. Yan, W. Wang, S. Chen, A. Viale, H. Zheng, J. H. Paik, C. Lim, A. R. Guimaraes, E. S. Martin, J. Chang, A. F. Hezel, S. R. Perry, J. Hu, B. Gan, Y. Xiao, J. M. Asara, R. Weissleder, Y. A. Wang, L. Chin, L. C. Cantley, R. A. DePinho, Oncogenic Kras maintains pancreatic tumors through regulation of anabolic glucose metabolism. *Cell* **149**, 656–670 (2012). doi:10.1016/j.cell.2012.01.058 Medline
65. P. Percipalle, E. Louvet, In vivo run-on assays to monitor nascent precursor RNA transcripts. *Methods Mol. Biol.* **809**, 519–533 (2012). doi:10.1007/978-1-61779-376-9_34 Medline
66. N. C. Jones, M. L. Lynn, K. Gaudenz, D. Sakai, K. Aoto, J.-P. Rey, E. F. Glynn, L. Ellington, C. Du, J. Dixon, M. J. Dixon, P. A. Trainor, Prevention of the neurocristopathy Treacher Collins syndrome through inhibition of p53 function. *Nat. Med.* **14**, 125–133 (2008). doi:10.1038/nm1725 Medline
67. T. Schmidt, M. Wiesbeck, L. Egert, T.-T. Truong, A. Danese, L. Voshagen, S. Imhof, M. Iraci Borgia, A. M. Deeksha, A. M. Neuner, A. Köferle, A. Geerlof, A. Santos Dias Mourão, S. H. Stricker, Efficient DNA- and virus-free engineering of cellular transcriptomic states using dCas9 ribonucleoprotein (dRNP) complexes. *Nucleic Acids Res.* **53**, gkaf235 (2025). doi:10.1093/nar/gkaf235 Medline
68. K. W. Orford, D. T. Scadden, Deconstructing stem cell self-renewal: Genetic insights into cell-cycle regulation. *Nat. Rev. Genet.* **9**, 115–128 (2008). doi:10.1038/nrg2269 Medline
69. M. Götz, A. Stoykova, P. Gruss, *Pax6* controls radial glia differentiation in the cerebral cortex. *Neuron* **21**, 1031–1044 (1998). doi:10.1016/S0896-6273(00)80621-2 Medline
70. M. Komada, H. Saitsu, M. Kinboshi, T. Miura, K. Shiota, M. Ishibashi, Hedgehog signaling is involved in development of the neocortex. *Development* **135**, 2717–2727 (2008). doi:10.1242/dev.015891 Medline
71. B. Yao, K. M. Christian, C. He, P. Jin, G. L. Ming, H. Song, Epigenetic mechanisms in neurogenesis. *Nat. Rev. Neurosci.* **17**, 537–549 (2016). doi:10.1038/nrn.2016.70 Medline
72. R. Schieweck, M. Götz, Pan-cellular organelles and suborganelles—from common functions to cellular diversity? *Genes Dev.* **38**, 98–114 (2024). doi:10.1101/gad.351337.123 Medline
73. N. S. Corsini, A. M. Peer, P. Moeseneder, M. Roiuk, T. R. Burkard, H.-C. Theussl, I. Moll, J. A. Knoblich, Coordinated control of mRNA and rRNA processing controls embryonic stem cell pluripotency and differentiation. *Cell Stem Cell* **22**, 543–558.e12 (2018). doi:10.1016/j.stem.2018.03.002 Medline
74. T. Rosenlehner, S. Pennavaria, B. Akçabozan, S. Jahani, T. J. O'Neill, D.

Krappmann, T. Straub, J. Kranich, R. Obst, Reciprocal regulation of mTORC1 signaling and ribosomal biosynthesis determines cell cycle progression in activated T cells. *Sci. Signal.* **17**, eadi8753 (2024). doi:10.1126/scisignal.adi8753 Medline
75. N. Savić, D. Bär, S. Leone, S. C. Frommel, F. A. Weber, E. Vollenweider, E. Ferrari, U. Ziegler, A. Kaech, O. Shakhova, P. Cinelli, R. Santoro, lncRNA maturation to initiate heterochromatin formation in the nucleolus is required for exit from pluripotency in ESCs. *Cell Stem Cell* **15**, 720–734 (2014). doi:10.1016/j.stem.2014.10.005 Medline
76. C. T. J. van Velthoven, T. A. Rando, Stem cell quiescence: Dynamism, restraint, and cellular idling. *Cell Stem Cell* **24**, 213–225 (2019). doi:10.1016/j.stem.2019.01.001 Medline
77. T. Moss, J. C. Mars, M. G. Tremblay, M. Sabourin-Felix, The chromatin landscape of the ribosomal RNA genes in mouse and human. *Chromosome Res.* **27**, 31–40 (2019). doi:10.1007/s10577-018-09603-9 Medline
78. P. C. Yelick, P. A. Trainor, Ribosomopathies: Global process, tissue specific defects. *Rare Dis.* **3**, e1025185 (2015). doi:10.1080/21675511.2015.1025185 Medline
79. E. Calo, B. Gu, M. E. Bowen, F. Aryan, A. Zalc, J. Liang, R. A. Flynn, T. Swigut, H. Y. Chang, L. D. Attardi, J. Wysocka, Tissue-selective effects of nucleolar stress and rDNA damage in developmental disorders. *Nature* **554**, 112–117 (2018). doi:10.1038/nature25449 Medline
80. E. Clough, T. Barrett, S. E. Wilhite, P. Ledoux, C. Evangelista, I. F. Kim, M. Tomashevsky, K. A. Marshall, K. H. Phillippy, P. M. Sherman, H. Lee, N. Zhang, N. Serova, L. Wagner, V. Zalunin, A. Kochergin, A. Soboleva, NCBI GEO: archive for gene expression and epigenomics data sets: 23-year update. *Nucleic Acids Res.* **52**, D138–D144 (2024). doi:10.1093/nar/gkad965 Medline
81. A. Danese, PhysiologicalGenomicBMC/TAPIR_Wiesbeck_et_al: v1.0.1 (v1.0.1), Zenodo (2026); https://doi.org/10.5281/zenodo.20067612.
82. J. Xu, Preparation, culture, and immortalization of mouse embryonic fibroblasts. *Curr. Protoc. Mol. Biol.* **Chapter 28**, 28.1 (2005). doi:10.1002/0471142727.mb2801s70 Medline
83. A. Grosche, A. Hauser, M. F. Lepper, R. Mayo, C. von Toerne, J. Merl-Pham, S. M. Hauck, The proteome of native adult Müller glial cells from murine retina. *Mol. Cell. Proteomics* **15**, 462–480 (2016). doi:10.1074/mcp.M115.052183 Medline
84. J. R. Wiśniewski, A. Zougman, N. Nagaraj, M. Mann, Universal sample preparation method for proteome analysis. *Nat. Methods* **6**, 359–362 (2009). doi:10.1038/nmeth.1322 Medline
85. J. G. Doench, N. Fusi, M. Sullender, M. Hegde, E. W. Vaimberg, K. F. Donovan, I. Smith, Z. Tothova, C. Wilen, R. Orchard, H. W. Virgin, J. Listgarten, D. E. Root, Optimized sgRNA design to maximize activity and minimize off-target effects of CRISPR-Cas9. *Nat. Biotechnol.* **34**, 184–191 (2016). doi:10.1038/nbt.3437 Medline
86. J. G. Doench, E. Hartenian, D. B. Graham, Z. Tothova, M. Hegde, I. Smith, M. Sullender, B. L. Ebert, R. J. Xavier, D. E. Root, Rational design of highly active sgRNAs for CRISPR-Cas9-mediated gene inactivation. *Nat. Biotechnol.* **32**, 1262–1267 (2014). doi:10.1038/nbt.3026 Medline
87. P. Grozdanov, O. Georgiev, L. Karagyozov, Complete sequence of the 45-kb mouse ribosomal DNA repeat: Analysis of the intergenic spacer. *Genomics* **82**, 637–643 (2003). doi:10.1016/S0888-7543(03)00199-X Medline
88. S. T. Jacob, Regulation of ribosomal gene transcription. *Biochem. J.* **306**, 617–626 (1995). doi:10.1042/bj3060617 Medline
89. J. Schindelin, I. Arganda-Carreras, E. Frise, V. Kaynig, M. Longair, T. Pietzsch, S. Preibisch, C. Rueden, S. Saalfeld, B. Schmid, J.-Y. Tinevez, D. J. White, V. Hartenstein, K. Eliceiri, P. Tomancak, A. Cardona, Fiji: An open-source platform for biological-image analysis. *Nat. Methods* **9**, 676–682 (2012). doi:10.1038/nmeth.2019 Medline
90. A. M. Bolger, M. Lohse, B. Usadel, Trimmomatic: A flexible trimmer for Illumina sequence data. *Bioinformatics* **30**, 2114–2120 (2014). doi:10.1093/bioinformatics/btu170 Medline
91. A. Dobin, C. A. Davis, F. Schlesinger, J. Drenkow, C. Zaleski, S. Jha, P. Batut, M. Chaisson, T. R. Gingeras, STAR: Ultrafast universal RNA-seq aligner. *Bioinformatics* **29**, 15–21 (2013). doi:10.1093/bioinformatics/bts635 Medline
92. P. Danecek, J. K. Bonfield, J. Liddle, J. Marshall, V. Ohan, M. O. Pollard, A. Whitwham, T. Keane, S. A. McCarthy, R. M. Davies, H. Li, Twelve years of SAMtools and BCFtools. *Gigascience* **10**, giab008 (2021). doi:10.1093/gigascience/giab008 Medline
93. S. Anders, P. T. Pyl, W. Huber, HTSeq—A Python framework to work with high-throughput sequencing data. *Bioinformatics* **31**, 166–169 (2015). doi:10.1093/bioinformatics/btu638 Medline
94. M. Lawrence, R. Gentleman, V. Carey, rtracklayer: An R package for interfacing with genome browsers. *Bioinformatics* **25**, 1841–1842 (2009). doi:10.1093/bioinformatics/btp328 Medline
95. Y. Zhang, G. Parmigiani, W. E. Johnson, *ComBat-seq*: Batch effect adjustment for RNA-seq count data. *NAR Genom. Bioinform.* **2**, lqaa078 (2020). doi:10.1093/nargab/lqaa078 Medline
96. M. I. Love, W. Huber, S. Anders, Moderated estimation of fold change and dispersion for RNA-seq data with DESeq2. *Genome Biol.* **15**, 550 (2014). doi:10.1186/s13059-014-0550-8 Medline
97. A. Liberzon, C. Birger, H. Thorvaldsdóttir, M. Ghandi, J. P. Mesirov, P. Tamayo, The Molecular Signatures Database (MSigDB) hallmark gene set collection. *Cell Syst.* **1**, 417–425 (2015). doi:10.1016/j.cels.2015.12.004 Medline
98. L. Käll, J. D. Canterbury, J. Weston, W. S. Noble, M. J. MacCoss, Semi-supervised learning for peptide identification from shotgun proteomics datasets. *Nat. Methods* **4**, 923–925 (2007). doi:10.1038/nmeth1113 Medline
99. P. Virtanen, R. Gommers, T. E. Oliphant, M. Haberland, T. Reddy, D. Cournapeau, E. Burovski, P. Peterson, W. Weckesser, J. Bright, S. J. van der Walt, M. Brett, J. Wilson, K. J. Millman, N. Mayorov, A. R. J. Nelson, E. Jones, R. Kern, E. Larson, C. J. Carey, İ. Polat, Y. Feng, E. W. Moore, J. VanderPlas, D. Laxalde, J. Perktold, R. Cimrman, I. Henriksen, E. A. Quintero, C. R. Harris, A. M. Archibald, A. H. Ribeiro, F. Pedregosa, P. van Mulbregt; SciPy 1.0 Contributors, SciPy 1.0: Fundamental algorithms for scientific computing in Python. *Nat. Methods* **17**, 261–272 (2020). doi:10.1038/s41592-019-0686-2 Medline
100. M. Martin, Cutadapt removes adapter sequences from high-throughput sequencing reads. *EMBnet. J.* **17**, 10–12 (2011). doi:10.14806/ej.17.1.200
101. T. Smith, A. Heger, I. Sudbery, UMI-tools: Modeling sequencing errors in Unique Molecular Identifiers to improve quantification accuracy. *Genome Res.* **27**, 491–499 (2017). doi:10.1101/gr.209601.116 Medline
102. F. Lauria, T. Tebaldi, P. Bernabò, E. J. N. Groen, T. H. Gillingwater, G. Viero, riboWaltz: Optimization of ribosome P-site positioning in ribosome profiling data. *PLOS Comput. Biol.* **14**, e1006169 (2018). doi:10.1371/journal.pcbi.1006169 Medline

## ACKNOWLEDGMENTS

We acknowledge the Core Facility Flow Cytometry (CF FlowCyt) at the Biomedical Center, Ludwig-Maximilians-Universität München, the Core Facility Protein Expression and Purification, the Core Facility Genomics and the Core Facility Metabolomics and Proteomics of the Helmholtz Center Munich for of the Helmholtz Institute Munich for providing equipment, services, and expertise.We thank Anthodesma Krontira, Judith Fischer-Sternjak and Reinhard Obst for helpful input. We also acknowledge Annita Achilleos, Chongbei Zhao and the Cellular, Tissue, & Molecular Biology Core at the Stowers Institute for Medical Research for their expertise and assistance. **Funding:** SHS acknowledges funding by the German Research Foundation (DFG STR 1385/5-1, STR 1385/9-1), the DFG networks SFB 1064 (project number 213249687) and Epiadapt (NI 1259/10-1), as well as the EU / EIC (European Innovation Council) project REGENERAR (Ref:101129812), and the Frontiers in Research Fund (NFRF) Transformation grant funded through three Canadian federal funding agencies (Canadian Institutes of Health Research, the Natural Sciences and Engineering Research Council of Canada and Social Sciences, and the Humanities Research Council of Canada), iNeuron. Research in the Trainor laboratory is supported by the Stowers Institute for Medical Research. JN acknowledges funding by TRR274/2 (ID 408885537), SPP 1738 "Emerging roles of non-coding RNAs in nervous system development, plasticity & disease", SPP1757 "Glial heterogeneity", the Fritz Thyssen Foundation, SPP2191 "Molecular mechanisms of functional phase separation" (ID 402723784, project number 419139133), SPP1935 "Deciphering the mRNP code: RNA-bound determinants of post-transcriptional gene regulation", Cellular Dynamics and Regulatory Pathways for Successful Regeneration (GO 640/19-1) and the Munich Cluster for Systems Neurology (SyNergy). FKM and ELA are supported by a Cancer Research UK

Programme Foundation Award (DRCPFA-Nov24/100005) to FKM. MD acknowledges funding (DFG, German Research Foundation)—TRR 387/1—514894665, DIP DI931/18-1 and DKH grant 70114554. MG acknowledges funding by the European Research Council (advanced grant NeuroCentro, 885382), by a New Frontiers in Research Fund Transformation grant to M.G., funded through three Canadian federal funding agencies (CIHR, NSERC, and SSHRC), by the German Research Foundation TRR274 (Nr. 408885537), EpiAdapt (GO 640/21-1), Cluster for Systems Neurology (EXC 2145 SyNergy-ID 390857198) and by the Impulse and Networking Fund of the Helmholtz Association (Helmholtz Excellence Network BioEM, grant EXNET-01-14). **Author contributions:** MW: formal analysis; validation; investigation; visualization; methodology; writing–original draft; writing–review and editing. LE and AD: data curation; formal analysis, methodology, writing–review. TTT, AK: methodology. MT, NC, SI, ELA, FKM, MIB, AK, LMCA, FV, AR, NFNM, EK, LB: investigation. RS: formal analysis, writing–review and editing SMH: formal analysis; validation; investigation; methodology. MD, FKM, PT, JN: Resources; supervision; funding acquisition; methodology; writing–review and editing. MG: Conceptualization; resources; supervision; funding acquisition; methodology; writing–review and editing. SHS: Conceptualization; resources; supervision; formal analysis, funding acquisition; methodology, writing–original draft; project administration; writing–review and editing. **Competing interests:** Authors declare that they have no competing interests. **Data, code, and materials availability:** Raw sequencing data are available on GEO (GSE324584) (*80*). All reproducibility code, processed files and proteomic data are available on Github (https://github.com/PhysiologicalGenomicBMC/TAPIR_Wiesbeck_et_al, https://doi.org/10.5281/zenodo.20054608) (*81*). All materials are available upon request from SHS. 

## SUPPLEMENTARY MATERIALS

science.org/doi/10.1126/science.aeh1348
Materials and Methods
Figs. S1 to S7
Tables S1 to S7
References (*82–102*)
MDAR Reproducibility Checklist

Submitted 12 March 2026; accepted 22 May 2026
Published online 2 July 2026
10.1126/science.aeh1348

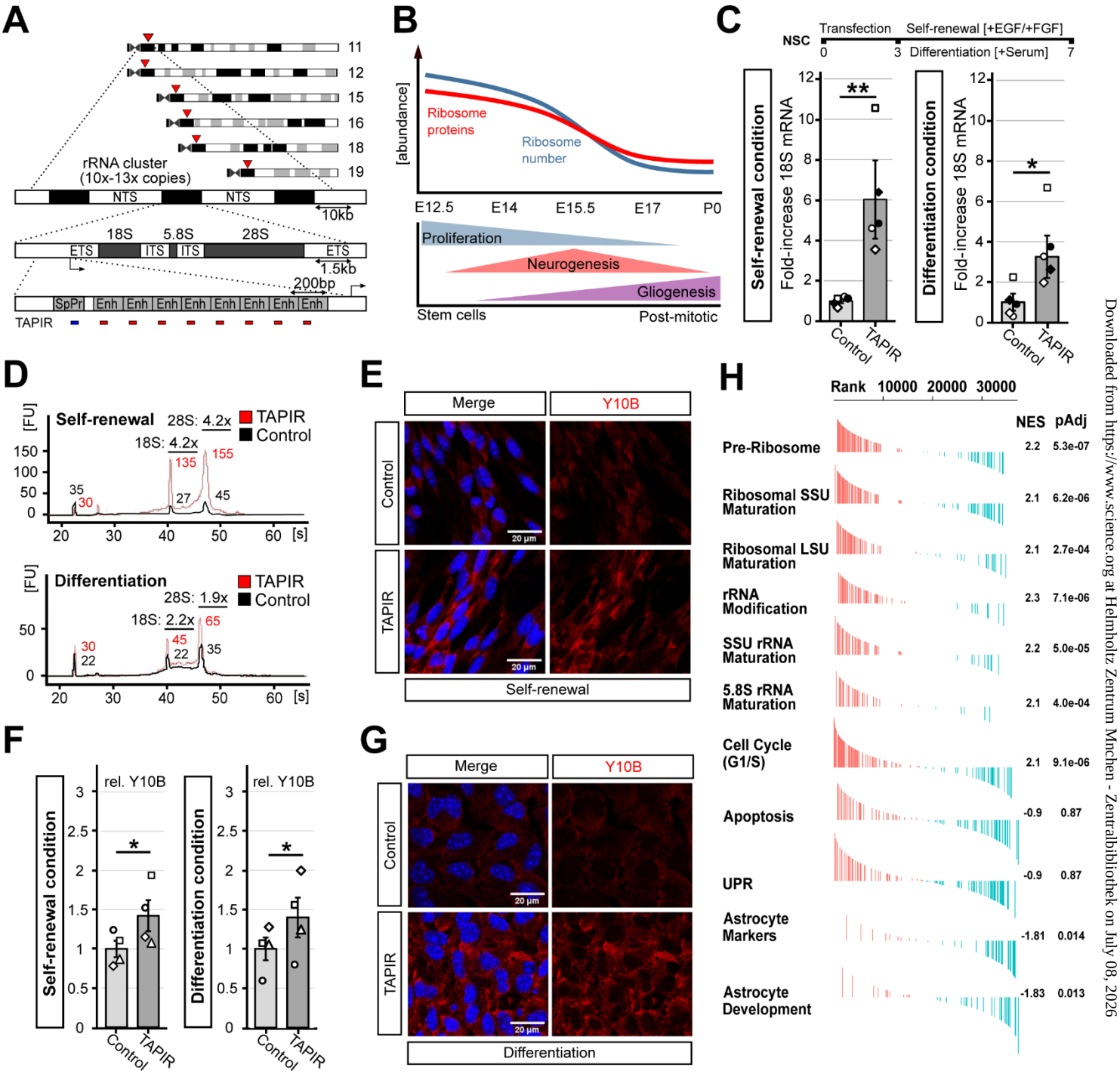

**Fig. 1. Activation of rRNA expression by TAPIR.** (**A**) Location and structure of rDNA cluster on mouse chromosomes highlighting TAPIR gRNA binding sites. (**B**) Scheme illustrating the decrease in ribosomal protein abundance and ribosome numbers during neural differentiation, based on (44). (**C**) (Top) Experimental outline for validating TAPIR-based activation of rRNA transcription in two media compositions, supporting NSC self-renewal and differentiation. (Below) RT-qPCR analysis of 18S rRNA expression induced by TAPIR, normalized to the housekeeper GAPDH (Bar graphs represent mean +/− SEM; symbols indicate biological replicates; n=5; White and black symbols distinguish independently prepared NSC lines and the use of alternative plasmid backbones. 18S – Self-renewal condition: ** p=0.00604; Mann-Whitney-Test; 18S – Differentiation condition: * p=0.01072; Mann-Whitney-Test). (**D**) Bioanalyzer profiles showing 18S and 28S transcript expression and size, with peak values for the internal marker and 18S/28S indicated. (TAPIR: Red; Control: Black) (**E** and **G**) Representative images (Scale bar: 50µm) and (**F**) quantification of Y10b immunocytochemistry after TAPIR or control treatment in two media conditions, supporting NSC self-renewal and differentiation. (Bar graphs represent mean +/− SEM; symbols indicate biological replicates; n=4; at least 120 cells per group have been analyzed. Y10B – Self-renewal: * p=0.03957; Paired T-Test, one-tailed; Y10B – Differentiation: * p=0.03716; Paired T-Test, one-tailed). (**H**) Gene ontology analysis of transcriptomic changes induced by TAPIR (Day 7; n=6; preparation and analysis described in the supplementary methods).

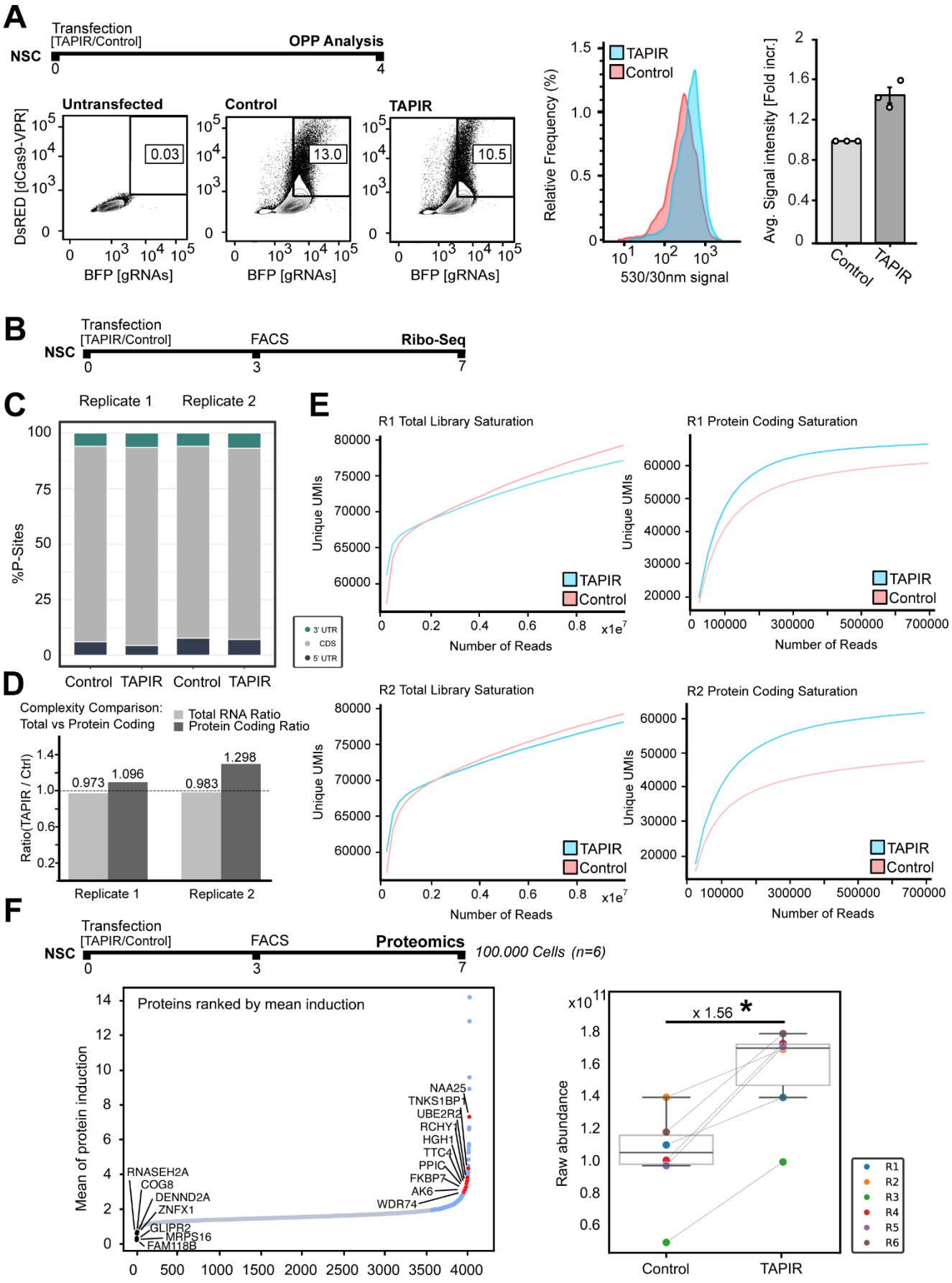

**Fig. 2. Quantification of translation rates after TAPIR-based rRNA activation.** (**A**) (Left) Scheme illustrating the experimental timeline for O-Propargyl-Puromycin (OPP) based quantification of nascent translation and an exemplary FACS analysis for selecting TAPIR-positive cells (DsRed: dCas9-VPR-construct; BFP: gRNA/Control-construct). OPP integration of newly synthesized proteins through a 5′FAM-Azide click-reaction enables quantitative measurement of translation rates by assessing the 530/30 signal at single-cell resolution. Histogram: Data are displayed using unit area normalization to allow comparison of fluorescence intensity independent of total event number. Bar Graph: 530/30 signal of TAPIR samples normalized to the corresponding control sample (Bars: mean of 3 biological replicates (circles); n=3). (**B**) Experimental timeline for Ribo-Seq. (**C**) The relative proportion (%) of ribosome P-site positions mapped to the 5′ untranslated region (5′UTR), coding sequence (CDS), and 3′ untranslated region (3′UTR) is shown for two independent Ribo-seq replicates. (**D**) Saturation plots of UMI counts from all reads (left) and mapping to protein coding genes (right) reveal more protected fragments in protein coding transcripts following TAPIR treatment in two biological replicates (Rep1,2). Additional quality control metrics and extended analyses are provided in fig. S2. (**E**) Quantification of (D). (**F**) (Top) Timeline of quantitative proteomics analysis, performed on day 7 post-transfection, normalized to 100,000 cells (n=6). (Below) Quantification of protein abundance of individual proteins averaged across all replicates (left) and of each individual replicate averaged across all proteins (right). (Left) Ranked normalized abundance calculated as the protein levels in TAPIR-treated mNSCs normalized to that in control-treated cells. Among 4022 detected proteins (with at least 3 values and with a minimum of 2 unique peptides), TAPIR treatment resulted in a proteome-wide increase of approximately 1.2-2.0 fold for over 3,800 proteins (Black: FC<0.75, Grey: 0.75 <= FC <= 2, Blue: FC >2). Notably, proteins (FC >3.0 fold) have roles in nucleolar structure, rRNA processing, and ribosomal protein maturation/assembly (highlighted in red). (Right) Proteome-wide analysis revealed a significant up-regulation of raw protein abundance in TAPIR-treated cells (Welch test; * p=0.013; n=6).

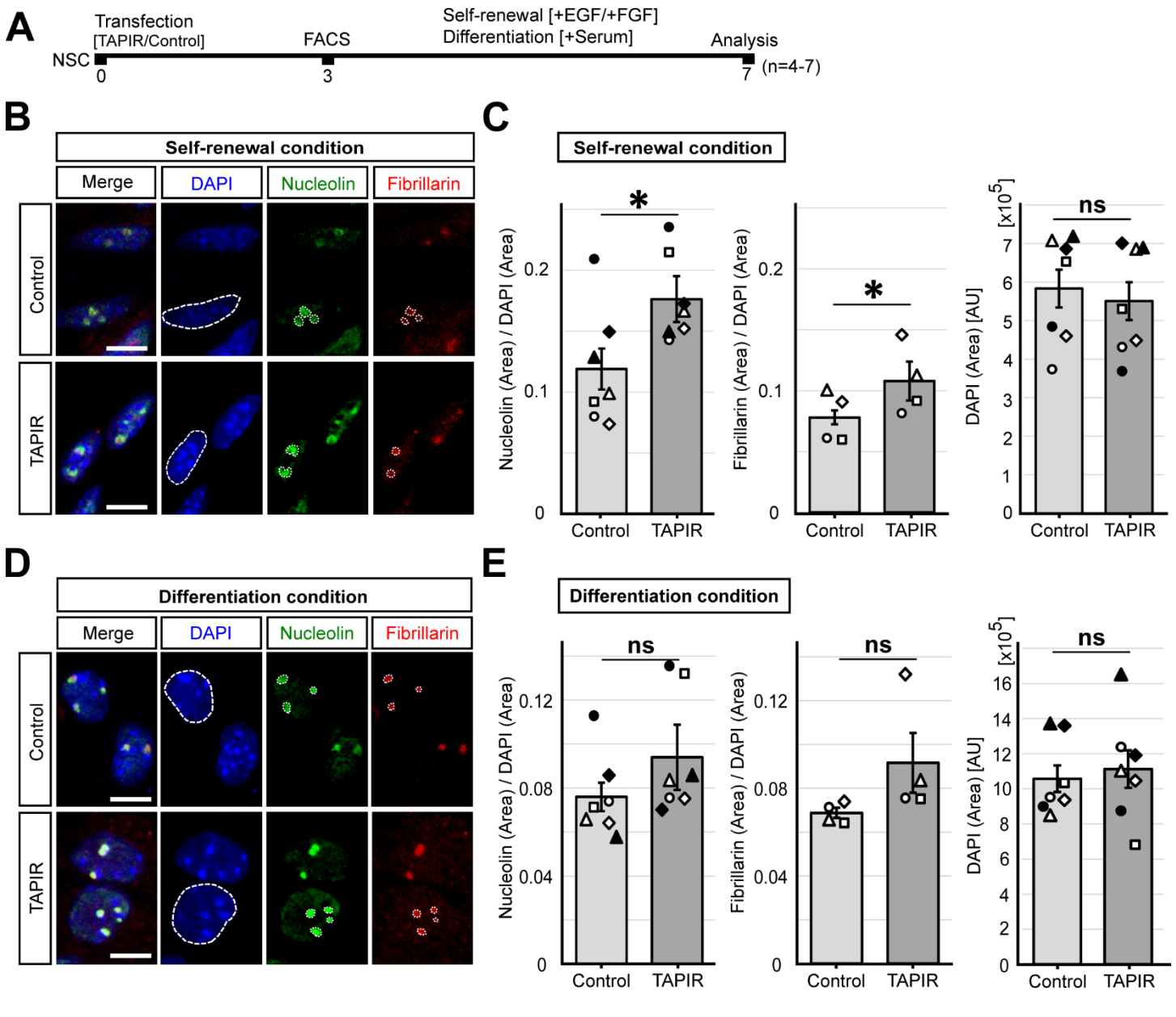


Fig. 3. TAPIR affects nucleoli size. (A) Experimental timeline of nucleoli quantification by immunohistochemistry. (B and D) Representative examples of immunocytochemistry measuring Nucleolin (Green) and Fibrillarin (Red). (Scale Bar: 10µm) (C and E) Total Nucleolin/Fibrillarin area per nucleus was measured and normalized to the nucleus area, measured by DAPI signal, under both self-renewal and differentiation condition (Bar graphs represent mean +/− SEM; Symbols indicate biological replicates; at least 240 up to 420 nucleoli per condition have been analyzed. Nucleolin: n=7; Self-renewal condition: * p=0.0257; Paired *t* test, two-sided; Differentiation condition: ns p>0.05; Paired *t* test, two-sided; Fibrillarin: n=4; Self-renewal condition: * p=0.00487; Paired *t* test, two-sided; Differentiation condition: ns p>0.05; Paired *t* test, two-sided; DAPI Area: n=7; Self-renewal condition: ns p=>0.05; Paired *t* test, two-sided; Differentiation condition: ns p>0.05; Paired *t* test, two-sided).

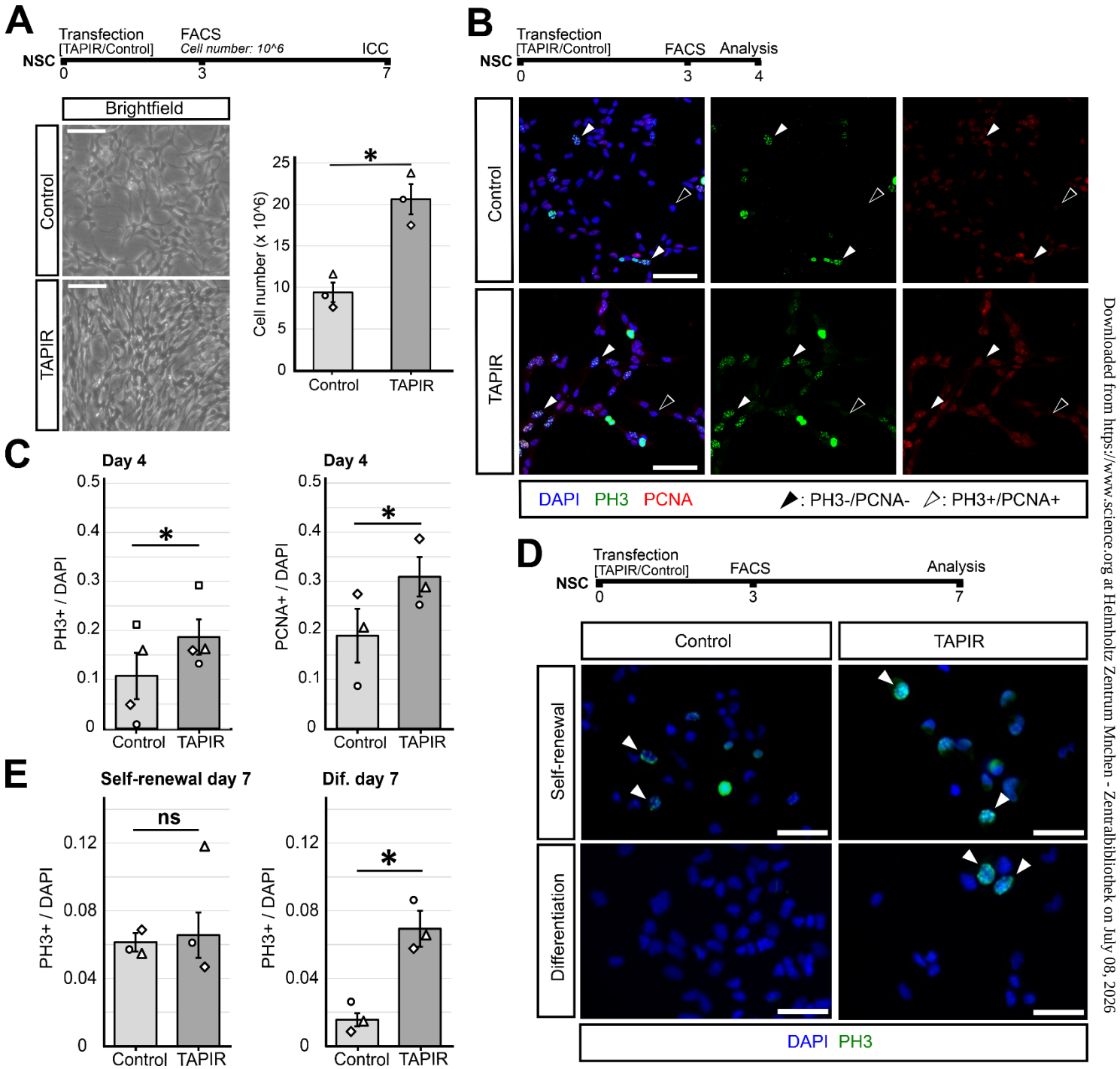

**Fig. 4. TAPIR treated mNSCs show more proliferative activity.** (**A**) (Top) Timeline of assessment of the proliferative capacity on day 7 post-transfection. One million TAPIR/control-expressing mNSCs were plated three days after construct delivery and cultured for an additional four days under proliferation conditions. (Left) Representative example of mNSCs after 4 days of expansion (day 7; Scale bar 50µm). (Right) Cell number quantification as metric for proliferative activity. Bright field images (scale bar: 50 µm) were taken and cells counted on day 7 (Bar graph represents mean +/− SEM; n=3; corresponding pairs from the same biological replicate are indicated by symbols; * p=0.0149; paired *t* test). (**B**) PH3- and PCNA-expression on day 4 in proliferation condition by immunohistochemistry (Black arrows indicate selected PH3 and PCNA negative cells; White arrows indicate selected PH3 and PCNA positive cells; Scale bar: 50µm; at least 600 cells per condition have been analyzed). (**C**) Quantification of PH3 and PCNA expression in TAPIR- /control-treated mNSCs (Bar graphs represent mean +/− SEM; Symbols indicate biological replicates; n=3-4; corresponding pairs from the same biological replicate are indicated; at least 600 cells per condition have been analyzed; PH3: * p=0.013; paired *t* test; PCNA: * p=0.038; paired *t* test). (**D**) PH3 expression on day 7 using immunohistochemistry (Arrows indicate selected PH3-positive cells; scale bar: 50 µm). (**E**) Quantification of PH3 expression in TAPIR-/control-treated mNSCs under self-renewal and differentiation conditions (Bar graphs represent mean +/− SEM; symbols indicate biological replicates; n=3; at least 350 up to 1200 cells per condition have been analyzed; corresponding pairs from the same biological replicate are indicated; Self-renewal: non-significant p>0.05; paired *t* test; Differentiation: * p=0.0098; paired *t* test).

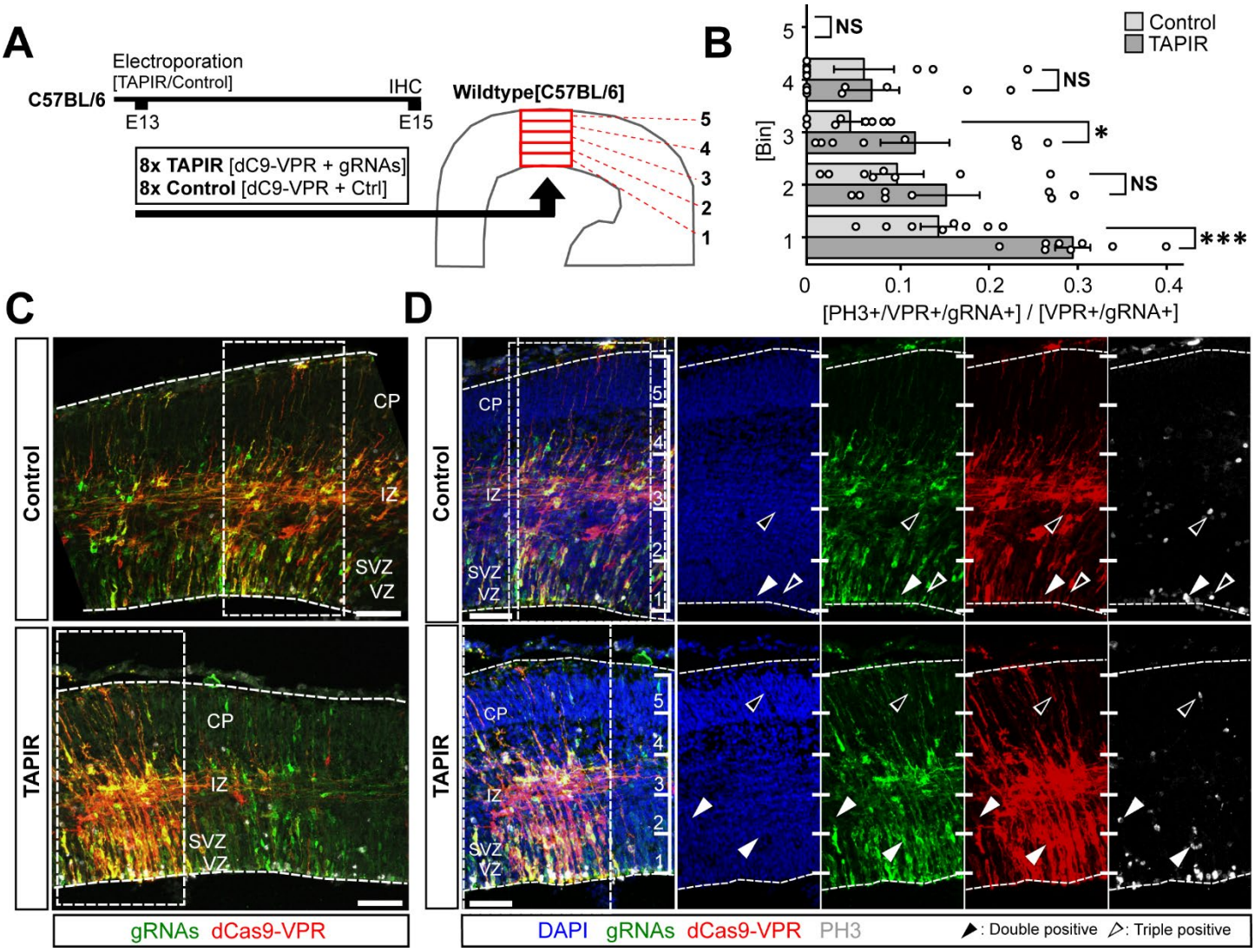


**Fig. 5. In utero electroporation (IUE) of TAPIR.** (**A**) TAPIR/control constructs were delivered to the cortices of C57BL/6 mice at embryonic day 13 (E13) via in utero electroporation (IUE). Mice were sacrificed at embryonic day 15 (E15), and their brains were analyzed by immunohistochemistry (n=8). (**B**) PH3 expression among successfully electroporated cells was quantified and normalized to the total number of electroporated cells. The cortex was subdivided into five bins, each representing 20% of the cortical area starting from the ventricle, and PH3 expression was analyzed based on these locations. (Bar graphs represent mean +/− SEM; circles indicate an embryonal brain analyzed; Bin 1: unpaired T-Test: *** p=0.0052; Bin 2: unpaired T-Test: non-significant; Bin 3: * unpaired T-Test: p=0.049; Bin 4: unpaired T-Test: non-significant; Bin 5: unpaired T-Test: non-significant). (**C**) In utero electroporation sites in E15 mouse cortices with indicated quantification areas (Square, dotted lines) and indicated cortex areas (CP: Cortical plate, IZ: Intermediate zone, SVZ: Subventricular zone, VZ: Ventricular zone). Expression dCas9-VPR is shown in red, gRNA expression in green. (**D**) In utero electroporation (dCas9-VPR: Red; gRNAs: Green) and PH3 IHC at E15. Selected double positive cells (PH3+/VPR+ or gRNAs+) are indicated by black arrows, selected triple positive cells (PH3+/VPR+/gRNAs+) are indicated by white arrows. Bins 1-5 and cortex areas are indicated (CP: Cortical plate, IZ: Intermediate zone, SVZ: Subventricular zone, VZ: Ventricular zone).

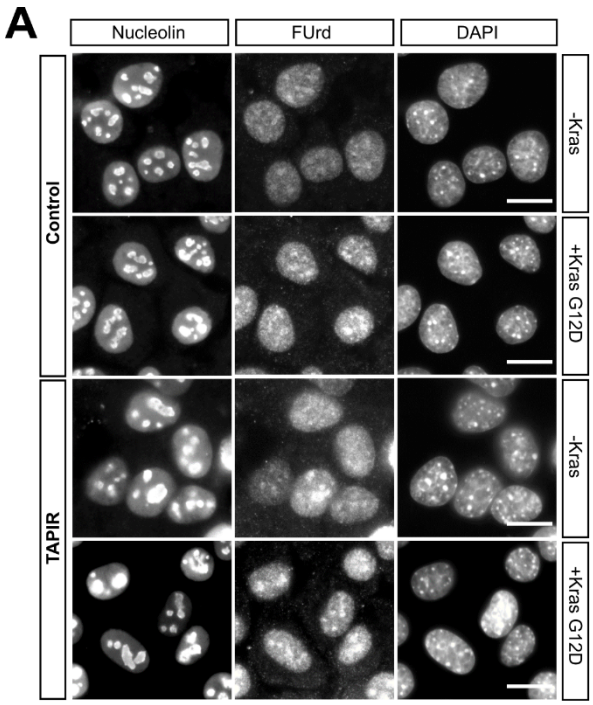


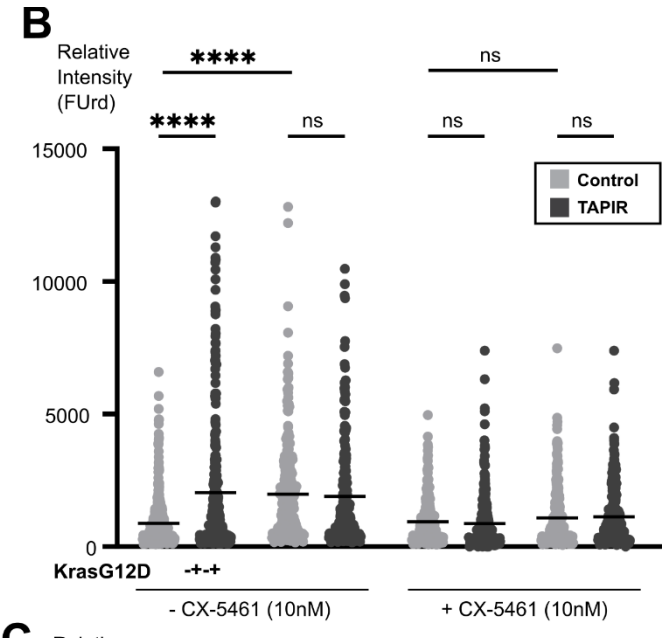


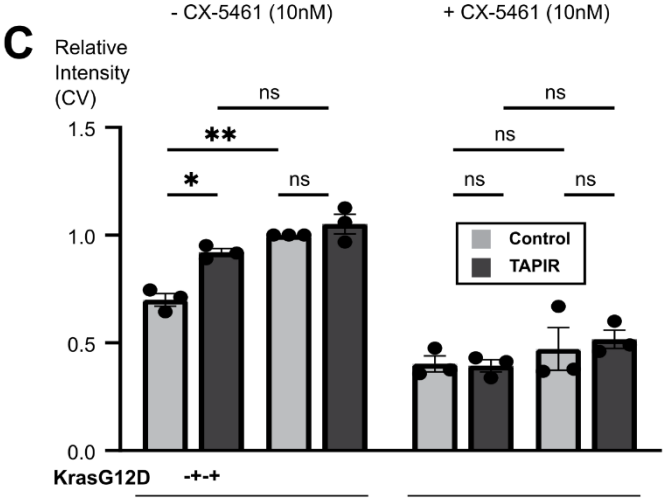


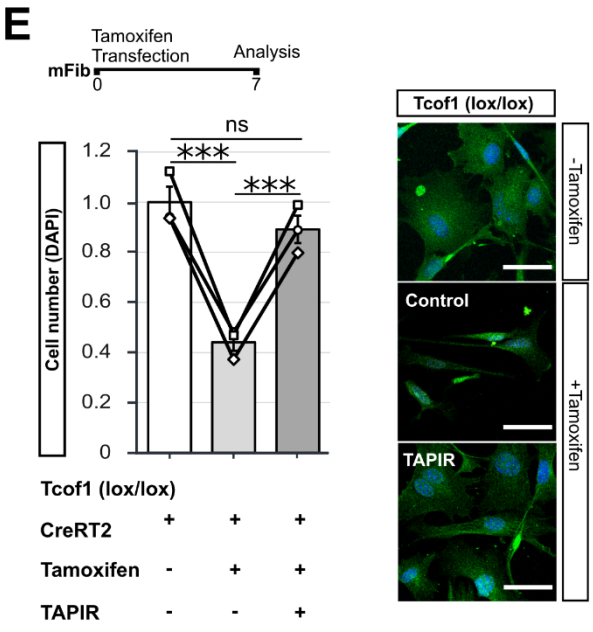


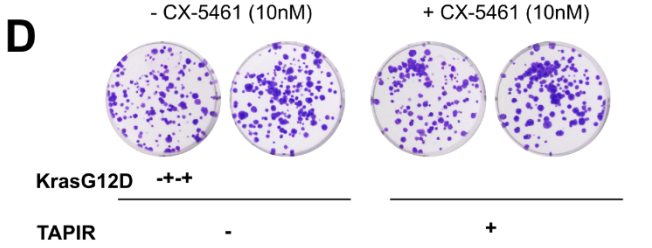


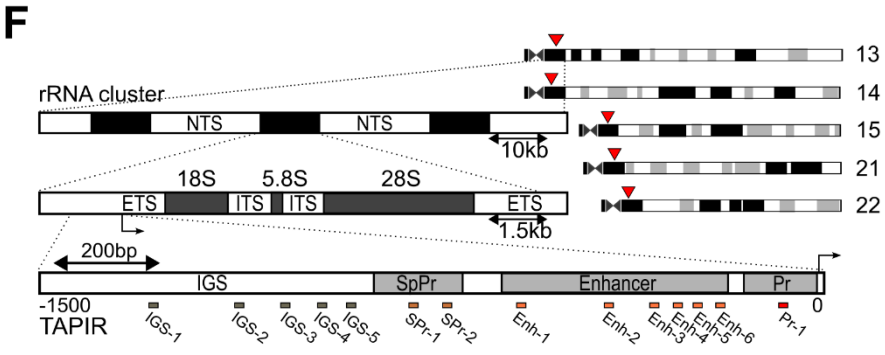


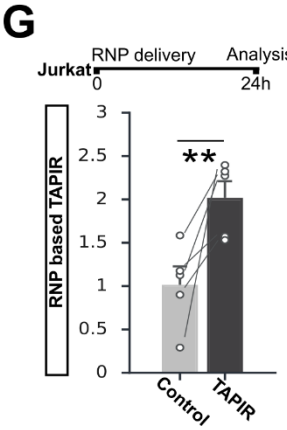

**Fig. 6. Application of TAPIR.** (**A** to **D**) TAPIR expressing or control PDAC cells were grown 48hrs with or without Doxycycline to induce oncogenic KRAS expression. (A) Representative immunocytochemistry pictures of PDAC cells after 48h of Doxycycline treatment showing Nucleolin, FUrd, and DAPI signals. (Scale Bar: 10µm). (B) Quantification of nucleolar FUrd intensity in PDAC (non-Doxycycline treated) cells as a measure of nascent rRNA levels shows TAPIR treatment is sufficient to increase rRNA expression over control-treated cells to a magnitude comparable to doxycycline-induced oncogenic KRAS expression. While TAPIR and oncogenic KRAS expression show comparable nucleolar FUrd induction, no additive effects were observed. CX-5461 treatment blocks oncogenic KRAS and TAPIR induced nucleolar FUrd signal (n=207-379 individual nucleoli from three biological replicates, **** p=<0.0001, *** p=0.0008, ** p=0.0024, ns: p=>0.1, Kruskal-Wallis test). (C) Quantification of Colony Formation 7 days after seeding. Colonies were visualized by crystal violet (CV). TAPIR treatment results in a significantly increased relative intensity of CV over non-induced control cells, similar to that observed by oncogenic KRAS-induction (n=3, ** p=0.0024, * p=0.0308, ns: p=>0.1, Ordinary one-way ANOVA). (D) Representative images of colony forming assays. (**E**) TAPIR rescues the consequences of *Tcof1* loss in Mouse Embryonic Fibroblasts. Deletion of *Tcof1* was induced by 4 day tamoxifen treatment of *Tcof1flx/flx;Cre-ERT2* mouse embryonic fibroblasts. (Left) Cell numbers were quantified on day 7 by counting DAPI-positive nuclei to evaluate treatment-dependent effects on cell survival (Paired *t* test, two-tailed; n=3; Tamoxifen- vs. Tamoxifen+/Control: *** p=0.0014; Tamoxifen+/Control vs Tamoxifen+/TAPIR: *** p=0.0005; Tamoxifen- vs Tamoxifen+/TAPIR: ns p=0.3076). (Right) Representative Immunocytochemistry pictures showing DAPI (Blue) and Vimentin (Green) (Scale Bar: 10µm). (**F**) Location and structure of rDNA multicopies on human chromosomes 13, 14, 15, 21, 22 highlighting TAPIR gRNA binding sites. A total of 14 gRNAs has been applied. (**G**) RNP-based induction of human 18S rRNA in Jurkat cells measured by qPCR 24h after RNP delivery (corresponding pairs from the same biological replicate are indicated by lines; ** p=0.00710; paired *t* test, two-sided).

# Manipulation of protein translation and stem cell self-renewal by CRISPR activation of rRNA transcription

Maximilian Wiesbeck, Emilie L. Alard, Florencia Merino, Niti Chowdhury, Luisa Egert, Anna Danese, Simon Imhof, Matilde Iraci Borgia, Akshaya Rajan, Nadine Fernandez-Novel Marx, Edina Kepesidis, Anna Köferle, Luis Miguel Cerron-Alvan, Franziska Vierl, Thi-Tram Truong, Manja Thorwirth, Lorina Bilalli, Jovica Ninkovic, Rico Schieweck, Markus Diefenbacher, Stefanie M. Hauck, Paul Trainor, Faraz K. Mardakheh, Magdalena Götz, and Stefan H. Stricker

*Science***Ahead of Print** DOI: 10.1126/science.aeh1348